

543238

IMPORTANT NOTICE: The current official version of this document is available via the Sandia National Laboratories WIPP Online Documents web site. A printed copy of this document may not be the version currently in effect.

Sandia National Laboratories
Waste Isolation Pilot Plant (WIPP)
Test Plan (TP)

Iron and Lead Corrosion in WIPP-Relevant Conditions, Test Plan TP 06-02

Rev. 1

Effective Date:

04/24/06

Prepared by:
Nathalie A. Wall
Repository Performance Dept. 6822
Sandia National Laboratories
Carlsbad, NM

David Enos
Corrosion & Electrochemical Science Dept. 1823
Sandia National Laboratories
Albuquerque, NM

WIPP:1.4.2.2:DC:QA-L:DPRP1:NF:TP 06-02, Rev. 1

APPROVAL PAGE

Authors:

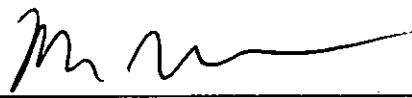


Nathalie A. Wall (6822) 04/12/06
Date



David Enos (6823) 4/17/06
Date

Technical Reviewer:



Martin Nemer (6821) 4/24/06
Date

ES&H Reviewer:



Ronald T. Parsons (6820) 4/13/06
Date

QA Reviewer :



Shelly Johnson (6820) 4-13-06
Date

Management Reviewer:



Mark Rigali (6822) 04/12/2006
Date

Information Only

TABLE OF CONTENTS

1 LIST OF FIGURES	5
2 LIST OF TABLES	6
3 DEFINITION OF ABBREVIATIONS AND ACRONYMS, AND INITIALISMS	7
4 REVISION HISTORY	9
5 PURPOSE AND SCOPE	10
6 INTRODUCTION	11
6.1 The Corrosion Process	12
6.2 Microbial Gases and Engineered Barrier Reactions in the WIPP	14
7 THERMODYNAMIC CALCULATIONS	16
7.1 Generalities	16
7.2 Fe Systems	18
7.2.1 Fe/H ₂ O System	19
7.2.2 Fe/H ₂ O/CO ₂ System	21
7.2.3 Fe/H ₂ O/H ₂ S System	22
7.2.4 Fe/H ₂ O/CO ₂ /H ₂ S System	24
7.3 Pb Systems	25
7.3.1 Pb/H ₂ O System	26
7.3.2 Pb/H ₂ O/CO ₂ System	27
7.3.3 Pb/H ₂ O/H ₂ S System	28
7.3.4 Pb/H ₂ O/CO ₂ /H ₂ S System	28
7.4 Summary of the Thermodynamic Calculations	29
7.5 Calculations Involving Microbial Gas Generation	30
7.5.1 Impact of Fe on Microbial Gases	31
7.5.2 Pb Impact on Microbial Gases	38
7.6 Summary of the Results of Interactions of Fe and Pb with Microbially Generated Gases	43
7.7 Additional Aspects on the Influence of Fe and Pb on the System	45
8 REVIEW OF DATA FOUND ON CORROSION IN THE WIPP	47
9 EXPERIMENTAL PROCESS DESCRIPTION	49
9.1 Materials	49
9.1.1 Alloys	49
9.1.2 Gas Composition	58
9.1.3 Presence of Organic Ligands in the Brine	59
9.2 Tasks List	60
9.2.1 Task 1: Brine Preparation	60

9.2.2 Task 2: Construction and Validation of a Mixed Flowing Gas Exposure System	63
9.2.3 Task 3: Software Qualification - Monitoring System and Software for the Mixed Flowing Gas Exposure System	70
9.2.4 Task 4: Evaluation of Carbonation of Fe in WIPP Internal Atmosphere and Likely Equilibrium Brines.....	72
9.2.5 Task 5: Evaluation of Carbonation of Pb in WIPP Internal Atmosphere and Likely Equilibrium Brines.....	73
9.3 Test Matrix.....	73
9.3.1 General Environmental Parameters	73
9.3.2 Materials to be Evaluated.....	74
9.3.3 Atmosphere	74
9.3.4 Brine Compositions	74
9.3.5 Sample Positioning	74
9.3.6 Experimental design.....	75
10 SAMPLE CONTROL – DATA QUALITY CONTROL	76
10.1 Sample Control	76
10.2 Data Acquisition Plan	76
10.3 Data Identification and Use	76
11 EQUIPMENT	77
11.1 Measuring and Test Equipment (M&TE).....	77
11.2 Weighing Equipment.....	77
11.3 Temperature Measuring Equipment	77
11.4 Liquid Measuring Equipment	77
11.5 Other Analytical Equipment	78
11.5.1 Ovens and Furnace.....	78
11.5.2 pH Meters and Autotitrators	78
11.5.3 Equipment for Chemical Analysis.....	78
11.5.4 Equipment for Mineralogical, and Textural Characterization	78
12 TRAINING	80
13 HEALTH AND SAFETY	81
13.1 Electrical	81
13.2 Chemical	81
13.2.1 General Chemical Compounds	81
13.2.2 Inert Gases	81
13.2.3 Hydrogen Sulfide	82
13.3 Thermal.....	85
13.4 Pressure	86
13.5 Readiness Review	86
14 PERMITTING/LICENSING	87
15 REFERENCES	88

1 LIST OF FIGURES

- Figure 1. Simplified view of the anodic and potential cathodic reactions for the corrosion process.....13
- Figure 2. N₂ gas circuit for the gas exposure system. This circuit includes the wet N₂ streams (top portion) as well as the dry N₂ streams. Also shown are two O₂ traps – a large capacity trap in the main supply line, and an indicating trap in one of the wet supply lines.....66
- Figure 3. Contaminant gas streams for the gas exposure system. Upper portion of the figure illustrates the CO₂ supply (equipped with O₂ traps similar to those described above). The lower portion illustrates the H₂S gas supply system – note that the supply gas for this leg is dry N₂ and as illustrated in Figure 2.....67
- Figure 4. Schematic representation of the gas flow streams passing into each of the four exposure chambers.....68
- Figure 5. Schematic representation of the gas composition analysis system. This system consists of a series of perma-pure gas dryers, a gas manifold (controlled by solenoid valves) to route the gas to each analyzer, and the two gas analyzers themselves.....69

2 LIST OF TABLES

Table 1. Abbreviations, Acronyms, and Initialisms.	7
Table 2. Standard Free Energies Selected by Brush (1990) and Chivot (2004).	19
Table 3. Free Energies Selected by the USGS (1995) and Chivot (2004).	26
Table 4. Result Summaries for Fe-Gas Reactions With the Denitrification And Sulfate Reduction Processes, but Without Methanogenesis.	33
Table 5. Summary of the Results for Fe-Gas Reactions With Denitrification, Sulfate Reduction, and Methanogenesis Processes, Case 1.	35
Table 6. Summary of Results for Fe-Gas Reactions with the Denitrification, Sulfate Reduction, and Methanogenesis Processes, Case 2.	37
Table 7. Summary of the Result of Pb-Gas Reactions with Denitrification and Sulfate Reduction Processes, and Without Methanogenesis.	39
Table 8. Result Summaries for Pb-Gas Reactions With Denitrification, Sulfate Reduction, and Methanogenesis Processes, Case 1.	41
Table 9. Result Summaries for Pb-Gas Reactions with Denitrification, Sulfate Reduction, and Methanogenesis Processes, Case 2.	43
Table 10. Percentage of Carbon Involved in the Microbial Gas Generation Reactions and Moles of Gases Generated from the Reactions between Metallic Fe and Pb and the Microbially Generated Gas.	45
Table 11. Materials of Construction for the Various Waste Containers.	50
Table 12. Material Compositions Defined by ASTM Specifications (all compositions in wt %).	53
Table 13. ASTM Specifications.	56
Table 14. Size and Number of the Pb-Lined Containers.	57
Table 15. Concentrations of Organic Ligands for a Homogeneous 10-Panel Repository.	60
Table 16. Compositions of GWB and ERDA-6 Prior to Equilibration with MgO.	61
Table 17. Compositions of GWB and ERDA-6 after Equilibration with MgO, in the Presence of Organic Ligands (Brush, 2005).	62
Table 18. Symptoms Observed after Different H ₂ S Exposure.	83

3 DEFINITION OF ABBREVIATIONS AND ACRONYMS, AND INITIALISMS

Table 1 defines the abbreviations, acronyms, and initialisms used within this Test Plan (TP).

Table 1. Abbreviations, Acronyms, and Initialisms.

Abbreviation or Acronym	Definition
ACGIH	American Conference of Governmental Industrial Hygienists
ASTM	American Society for Testing and Materials
CO ₃ ²⁻	carbonate ion
CH	contact handled
CH ₄	methane
CPR	cellulosic, plastic, and rubber
CO ₂	carbon dioxide
DOE	Department of Energy
EDTA	ethylenediaminetetraacetic acid
ERDA-6	Energy Research and Development Administration (WIPP Well) 6. Synthetic Castile Formation brine
ES&H	Environmental Safety and Health
Fe	elemental (metallic) iron
FMT	Fracture-Matrix Transport, a geochemical speciation and solubility code
GWB	Generic Weep Brine, a synthetic Salado Formation brine.
H ₂	hydrogen gas
H ₂ S	hydrogen sulfide
HSLA	high-strength, low-alloy
ICP-OES	Inductively-coupled plasma-optical emission spectrometer
LC50	Lethal concentration for 50% of humans
m	molal (mol/kg)
M	molar (mol/L)
M&TE	measuring and test equipment

Table 1. Abbreviations, Acronyms, and Initialisms. (cont.)

Abbreviation or Acronym	Definition
MSDS	Material Safety Data Sheet
N ₂	nitrogen gas
NHE	normal hydrogen electrode
NP	(SNL WIPP) Nuclear Waste Management (QA) Procedure
O ₂ (g)	oxygen gas
OSHA	Occupational Safety and Health Administration
PA	performance assessment
Pb	elemental lead
PEL	permissible exposure limit
Pu	plutonium
QA	quality assurance
PABC	(WIPP) performance assessment baseline calculations
PPE	personal protection equipment
RH	remote handled
sccm	Standard cubic centimeters per minute (i.e., milliliters per minute)
SNL	Sandia National Laboratories
SOP	Standard Operating Procedure
SP	(SNL WIPP) Activity/Project Specific Procedure
S ²⁻	sulfide ion
TP	test plan
TVL	Threshold Limit Value
TRU	Transuranic
WIPP	Waste Isolation Pilot Plant
XRD	X-ray diffractometer

4 REVISION HISTORY

This is the first revision of this TP. This revision includes a detailed section addressing the Environmental Safety and Health (ES&H) concerns that this work might raise.

Subsequent versions will be prepared in accordance with the following Sandia National Laboratories (SNL) Waste Isolation Pilot Plant (WIPP) Quality Assurance (QA) Procedures: NP 6-1, NP 6-2, and NP 20-1 (Subsection 5.2).

Information Only

5 PURPOSE AND SCOPE

This document describes the experimental work that will be performed to assess the corrosion behavior of carbon steel and lead (Pb) alloys used to contain contact handled (CH) and remote handled (RH) waste under WIPP-relevant conditions. More specifically, the objective is to determine to what extent the aforementioned materials consume carbon dioxide (CO₂) through the formation of carbonates, potentially supporting magnesium oxide (MgO) in its role of CO₂ sequestration; MgO is the WIPP engineered barrier, chosen to mitigate the effect of microbial CO₂ generation on actinide mobility in a post-closure repository environment and to buffer brine pH at a moderately basic level, thus minimizing the solubilities of actinides in WIPP brines. Furthermore, the rate at which the waste-container materials consume other microbially-produced gasses, such as hydrogen sulfide (H₂S), within the post closure WIPP environment will also be explored. The design of the overall test system, as well as the applicable calculations (brine composition, likely corrosion product compositions, etc.) are also presented.

The work proposed in this document can be loosely broken down into three stages. The first stage will be the acquisition, assembly, and calibration of the equipment as well as the production of the software interface necessary to conduct the test themselves. This is anticipated to take three months, barring any unanticipated delays. The second stage of the work is the execution of the experiments defined in this document, and will continue for a period of two years. The analysis and official documentation of the results will be the third and final stage of the program. In this portion, the quantity and nature of any carbonates which form, along with the general electrochemical behavior of each material will be documented. A final report will be generated and submitted to DOE at the end of this stage, which is anticipated to take approximately 3 months. Once complete, the results of this study will provide considerable insight into the extent to which the metals within the WIPP (specifically iron and lead) might augment the actions of the engineered barrier through the consumption of carbon dioxide.

6 INTRODUCTION

The WIPP is a repository for transuranic (TRU) wastes, located within the bedded salts of the Permian Salado Formation. This formation consists of an interbedded halite-and-anhydrite formation overlaying the Castile Formation. The repository will consist of eight seven-room panels upon completion. Additionally, there are two access drifts in the waste region that will also be available for waste disposal and will constitute two supplementary panels. The WIPP performance assessment (PA) analyzes the performance of the repository, including the consequences of future inadvertent human intrusions into the repository by drilling for resources; such intrusions could lead to a postulated release of radionuclides to the accessible environment before the end of the 10,000-year regulatory period. To accomplish this, the U.S. Department of Energy (DOE) has examined different drilling scenarios, which involve the penetration of the repository by one or more drill holes; some of the scenarios also involve the possibility of the penetration of a pressurized Castile brine reservoir (U.S. DOE, 2004. Chapter 6). The estimated quantity of radionuclides released to the accessible environment following penetration of the repository depends on the chemistry of these radioelements. As an example, consider plutonium (Pu), which is less soluble when it speciates in lower oxidation states, such as Pu(III) and Pu(IV), than in higher oxidation states, such as Pu(VI). Thus it follows that in order to minimize the release of such radionuclides from the repository, it is desirable to maintain all such species in their least-soluble form (i.e., low oxidation states).

The nature of the environment within the WIPP following closure will, to a large extent, control the speciation of the radionuclides within the waste. More specifically, there are components contained within the waste that can impact the oxidative or reductive nature of the environment, such as the metals undergoing active corrosion. If the metals undergo active corrosion within the WIPP, the corrosion process will serve to maintain electrochemically reducing conditions. The predominant metals within the WIPP will be iron (Fe) and Pb, present within the waste itself, as well as the containers used to hold the waste until emplacement. The current inventory predicts that 280 and 599 kg/m³ of Fe and Fe-base alloys will be present in the CH and RH wastes, respectively. Also, 0.013 and 420 kg/m³ of Pb will be present in the CH and RH wastes, respectively. The corrosion behavior of these materials, specifically the kinetics of the corrosion reaction, will be controlled by the availability of water (in brine) at the metal surface, as well as the internal atmosphere within the WIPP. It should be noted that if the corrosion process is stifled, for example due to passivation of the metal surfaces, electrochemically reducing conditions will no longer be maintained by the corrosion process.

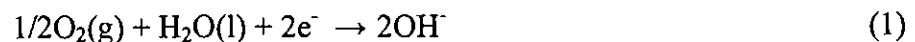
In addition to Fe and Pb, the waste disposed within the WIPP contains significant quantities of cellulosic, plastic, and rubber (CPR) materials. With time, microbial activity may consume some portion of the CPR materials, resulting in the generation of significant quantities of CO₂, H₂S, hydrogen (H₂), nitrogen (N₂), and methane (CH₄). Some of these gasses, namely CO₂ and H₂S, may interact with the metallic Fe and Pb, altering their electrochemical behavior. Elevated concentrations of both gasses have been demonstrated to passivate Fe under certain conditions (Telander and Westerman, 1993; 1997). If the Fe and Pb within the WIPP passivate, they will no longer contribute to maintaining the reducing environment within the WIPP through the corrosion process. Under these conditions, Fe and Pb would not be available to prevent oxidation of the radionuclides, although other reductants may still be available.

The sections below provide a brief introduction to the corrosion process, as well as detail the potential microbial activity and reaction pathways within the WIPP.

6.1 The Corrosion Process

Corrosion is the destructive attack of a metal by chemical or electrochemical reaction with its environment. (For a more complete discussion, see Uhlig and Revie, 1985) In this study, we are concerned with the corrosion of Fe- and Pb-base alloys under WIPP-relevant environmental conditions. More specifically, this study will focus on the products of the corrosion process and their implications for the TRU components within the waste. This section will provide a very basic description of the corrosion process. A more complete discussion is beyond the scope of this section, but can be found in the text referenced above.

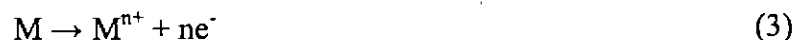
Broadly speaking, the corrosion reaction may be broken down into two components: the anodic reaction (oxidation) and the cathodic reaction (reduction). The anodic reaction is typically metal oxidation, while the cathodic reaction can include processes such as oxygen (O₂) reduction, water reduction, etc. An important concept here is that the sum of all the anodic reactions (i.e., total oxidative current) must be equal to the sum of all cathodic reactions (i.e., total reductive current); changes in one will have an equal impact on the other. As an example, consider the transition from an O₂-containing environment to one where O₂ has been depleted. In an O₂-rich environment, the cathodic reaction is typically O₂ reduction:



If the total supply of O₂ is limited (as will be the case in the WIPP upon closure), O₂ will become depleted with time, and thus the rate of the reaction will become concentration limited, eventually becoming negligible in magnitude. At this point, if no other viable cathodic reactions were available, the anodic reaction would also stop, as there would be no cathodic reaction to support it. However, in an aqueous environment, there are other cathodic reactions that could take place, such as water reduction;



This transition from O₂ reduction as the primary cathodic reaction to water reduction as the O₂ concentration is depleted is illustrated in Figure 1. Three reactions are shown in the figure, the anodic reaction (metal oxidation), expressed as:



and the two cathodic reactions we are concerned with here, O₂ reduction and water reduction. As the rate of the reaction increases, O₂ reduction transitions from a charge transfer-controlled reaction to a mass transport-controlled process; its maximum rate is limited by how quickly dissolved O₂ can get to the metal surface. (i.e., as the cathodic overpotential is increased, the rate of O₂ reduction can not similarly increase, as it is already consuming all of the dissolved O₂ as it reaches the metal surface). As the O₂ concentration decreases, so does the limiting current density for the O₂ reduction.

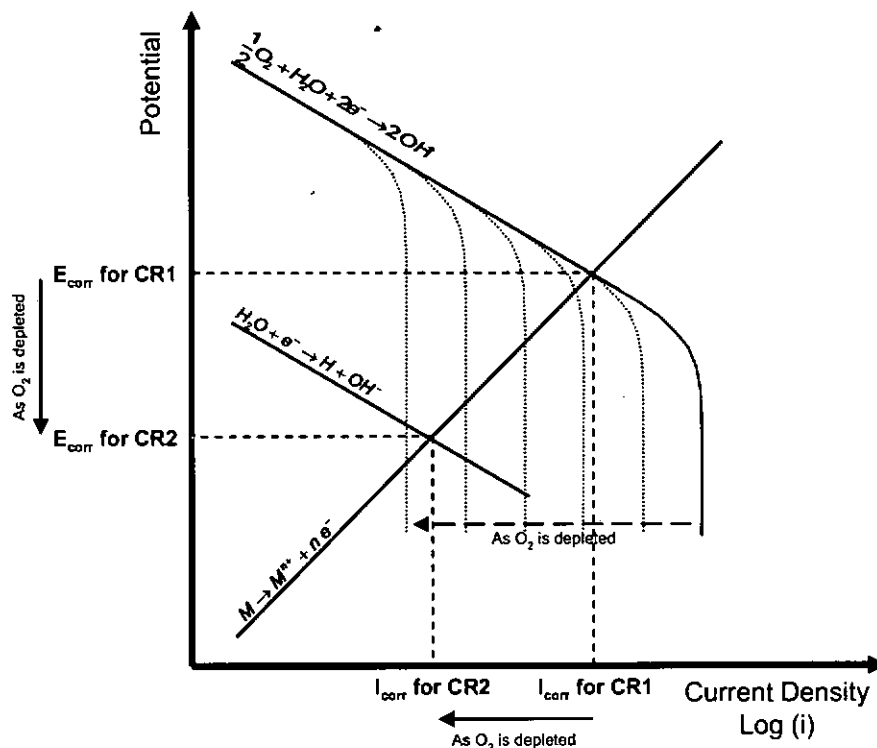


Figure 1. Simplified view of the anodic and potential cathodic reactions for the corrosion process.

As discussed above, the total anodic rate will be equal to the total cathodic rate. In the figure, that rate is the point at which the anodic and cathodic curves cross. (Note that the anodic and cathodic electrode areas are important here, as the total current is equal to the total active area for each process multiplied by the current density) In the figure, the rate of the cathodic and anodic reactions will initially be equal to the value of I_{corr} for CR1. As the O_2 concentration decreases, the limiting current for O_2 reduction decreases, resulting in the shift shown in the figure. Eventually, another cathodic reaction (in this case, water reduction) can become thermodynamically viable, and it will then dictate the total anodic and cathodic reaction rates (indicated by I_{corr} for CR2).

In the context of this study, a number of other cathodic reactions may become operative. Due to the potential for an elevated concentration of CO_2 , another potential cathodic reaction is the direct oxidation of H through the $\text{H}_2\text{CO}_3/\text{HCO}_3^-$ equilibrium:



It has also been suggested that in CO_2 solutions at elevated pH (i.e., >5), the direct oxidation of the hydrogen ion through the $\text{HCO}_3^-/\text{CO}_3^{2-}$ equilibrium could become important (Nordsveen, 2003):



Furthermore, the presence of CO₂ in significant quantities can also result in the formation of iron carbonate (FeCO₃(s)) through the reaction:

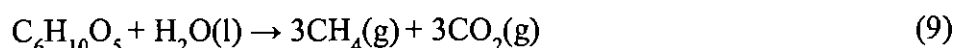
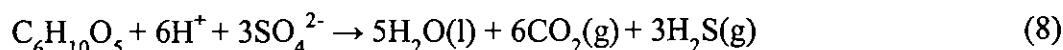
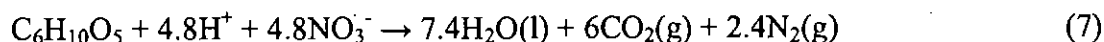


If the FeCO₃ forms as a sufficiently dense film on the Fe surface, it could potentially result in passivation. However, as will be illustrated below in section 7.2.4, the presence of H₂S which will likely accompany the CO₂ (see section 6.2 below) will tend to destabilize this film, preventing passivation due to carbonate formation.

There are a number of factors that will impact the rate and overall nature of the corrosion process. As with chemical reactions, electrochemical reactions are impacted by the environmental conditions under which they take place. These include the local environment at the metal-solution interface (i.e., composition, pH, etc.), temperature, availability of O₂ or other reducible species, etc.

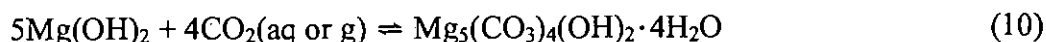
6.2 Microbial Gases and Engineered Barrier Reactions in the WIPP

Microbial activity, if it occurs to a significant extent in the WIPP, will consume CPR materials by one or more of the following reactions (Brush, 1990; Francis and Gillow, 1994; Brush, 1995; Wang and Brush, 1996; Francis and Gillow, 1997):



As a result of microbial activity via these reactions, significant quantities of gases could be generated - in particular CO₂(g).

The microbially generated CO₂(g) will then react with the MgO, the WIPP engineered barrier. Laboratory and modeling studies have shown that the carbonation reaction (Equation (10)) of MgO will buffer f_{CO₂} at a value of 10^{-5.50} atm in WIPP brines (DOE, 2004, Appendix BARRIERS), where Mg(OH)₂ is the main hydration product of the mineral periclase (MgO) expected in the WIPP and Mg₅(CO₃)₄(OH)₂·4H₂O is the form of the mineral hydromagnesite predicted by the repository models.



Moreover, the brucite-dissolution reaction, described in Equation (11), will buffer pH in the WIPP at a value of 8.69 in Generic Weep Brine (GWB) and 9.02 in Energy Research and Development Administration (WIPP Well) 6 Synthetic Castile Formation brine (ERDA-6), where ERDA-6 represents fluids from reservoirs in the Castile Formation and GWB represents

intergranular brines from the Salado Formation at or near the stratigraphic horizon of the repository. (DOE, 2004, Appendix BARRIERS)



The large quantities of Fe and Pb present in WIPP may also contribute to the consumption of the microbially generated gases, primarily through the formation of carbonates (CO_3^{2-}) and sulfides (S^{2-}). After the limited concentration of O_2 trapped within the repository at the time of closure is depleted via the corrosion process and the aerobic microbial consumption of CPR materials, anoxic corrosion of Fe and Pb will occur (Brush, 1990). WIPP-specific experiments (Telander and Westerman, 1993; 1997) verified Brush's (1990) hypothesis that carbon steels will corrode under such conditions. A more thorough discussion of their results, along with several similar studies, is presented in Section 8 of this document.

7 THERMODYNAMIC CALCULATIONS

In the following sections, a series of thermodynamic calculations are performed to assess the potential Fe and Pb compounds that might form under WIPP-relevant conditions. Following the thermodynamic calculations is a discussion of their implications in terms of interactions of both Fe and Pb with the gas compositions likely to result from microbial activity within the WIPP.

A number of key assumptions were made prior to conducting these calculations. First, these calculations illustrate the phases that are most stable thermodynamically; they provide no information on the kinetics of the formation process or the formation of any metastable phases produced prior to the potential conversion to the most thermodynamically stable state (i.e., reaction pathways other than direct production of the most thermodynamically stable state). In addition, for simplicity, all of these calculations were performed assuming that the environment was essentially pure water with only the reactive species of interest (i.e., carbon and sulfur) being present. As such, they may or may not indicate what might exist within a brine, which will contain, among other things, up to 5 M chloride. It is possible that the impact of the omitted species will dominate the actual behavior of the system, rendering the results discussed below partially or completely invalid. Thus it is critical that the reader understand that the calculations made in the following sections only provide an indication as to whether or not something might happen; they are not conclusive evidence that a given phase, such as FeCO_3 , will or will not form.

7.1 Generalities

The chemical equilibrium, in which b mol of B reacts with c mol of C to produce d mol of D and e mol of E is expressed as Equation (12):



Phase designators immediately follow the chemical formula and appear in parenthesis: (l) for liquid, (aq) for aqueous, (g) for gas, and (s) for solid. The designators "cr" and "am" are used for solid in crystalline and amorphous phases, respectively.

The thermodynamic equilibrium constant of reaction 12 is expressed as:

$$K = \frac{\{D\}^d \times \{E\}^e}{\{B\}^b \times \{C\}^c} \quad (13)$$

where $\{X\}$ is the activity of X and is expressed as:

$$\{X\} = [X] \times \gamma_X \quad (14)$$

where $[X]$ is the concentration of X and γ_X the activity coefficient of X.

Equilibrium constants involving a solid compound as the reactant and nonsolid species as products are denoted as solubility products. An example of such an equilibrium and its associated solubility product are presented below:



The term "standard state," often used in thermodynamics, defines a baseline of behaviors. The standard state pressure is 1 atm. The standard state of a gaseous substance is defined as the pure gaseous substance at the standard-state pressure, in which it behaves as an ideal gas; for a liquid, it is the pure liquid at the standard-state pressure; for a solid, it is the pure solid at the standard-state pressure; and for a solute X in solution, it is a liquid solution at the standard-state pressure and in which the molality of X is 1 mol of solute per kg of solvent and its activity coefficient is 1.

The standard free energy of a chemical reaction is the difference between the sum of the free energies of formation of the products in their standard states and the sum of the free energies of formation of the reactants in their standard states:

$$\Delta G_R^0 = \Delta G_f^0 \text{ products} - \Delta G_f^0 \text{ reactants} \quad (16)$$

The standard free energy of the equilibrium is also related to the thermodynamic equilibrium constant, as shown in the following equation:

$$\Delta G_R^0 = -R \times T \times \ln(K) = -R \times T \times \ln(10) \times \log(K) \quad (17)$$

where R is the gas constant (8.3145 J/mol K) and T the absolute temperature.

Redox reactions are usually expressed in terms of their electrode (half-cell) potential E_h , given as reduction potentials relative to the standard hydrogen electrode. The standard electrode potential E_h^0 is the potential relative to the standard hydrogen electrode, when all the components are in their respective standard state. The general equation for a half-cell reaction:



where O and R are the oxidized and reduced species of a specific entity, respectively (e.g. Fe(III) vs. Fe(II)) and n is the number of electrons involved in the reaction. The Nernst equation is the expression of the electrochemical potential of the redox reaction:

$$E_h = E_h^0 + \frac{R \times T}{n \times F} \times \ln \left(\frac{\{R\}^r \times \{C\}^c}{\{O\}^o \times \{B\}^b} \right) \quad (19)$$

where F is the Faraday constant, 96485 C/mol. E_h may also be expressed as a function of the free energy of the thermodynamic equilibrium:

$$E_h = -\frac{\Delta G_R}{n \times F} \quad (20)$$

Visualization of the region of predominance for the different species of a system is quite important to predict the species encountered at specific conditions. A plot of the electrochemical potential of the chemical, electrochemical, and redox reactions as a function of pH, commonly referred to as a Pourbaix diagram, allows the prediction of the most thermodynamically stable species as a function of the electrochemical conditions that exist within the system. Note, however, that this diagram is based entirely on thermodynamic data, and as such does not provide any kinetic information (e.g., rates of reaction, presence of metastable phases, etc.) Several examples of Pourbaix diagrams are presented throughout this document. As each of the chemical and electrochemical reactions represented on the diagram are a function of concentration, for all instances in this paper they will be presented at a concentration of 10^{-6} M.

7.2 Fe Systems

Metallic Fe will oxidize in water at 25 °C and 1 atm. This oxidation results in the formation of a number of solid corrosion products, including $\text{Fe}(\text{OH})_2(\text{s})$, $\text{Fe}(\text{OH})_3(\text{s})$, $\text{Fe}_2\text{O}_3(\text{s})$, and $\text{Fe}_3\text{O}_4(\text{s})$. In solution, Fe typically exhibits two oxidation states, Fe(II) (ferrous) and Fe(III) (ferric). The standard potential for the couple $\text{Fe}^{2+}/\text{Fe}^{3+}$ is 0.771 V.

Brush (1990) conducted a series of thermodynamic calculations and estimated the amount of gas generated by the corrosion of Fe by H_2O , CO_2 , and H_2S . In the following text, his results are compared to similar calculations performed using Chivot's (2004) selection of thermodynamic data. Because of the reducing conditions within the WIPP, only the thermodynamic functions of Fe(II) will be considered. The standard free energies of formation selected by Brush (1990) and Chivot (2004) are included in Table 2. All values are expressed in kJ/mol (where 1 kJ/mol is equivalent to 4.184 J/cal.)

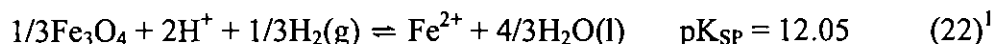
Table 2. Standard Free Energies Selected by Brush (1990) and Chivot (2004).

Compound	ΔG_f^0 selected by Brush (1990) (kcal/mol)	ΔG_f^0 selected by Brush (1990) (kJ/mol)	ΔG_f^0 selected by Chivot (2004) (kJ/mol)
H ₂ O(l)	-56.6781	-237.1	-237.140
H ₂ (g)	0	0	0
H ⁺	0	0	0
CO ₂ (g)	-94.2579	-394.4	-394.373
H ₂ S(g)	-8.017	-33.54	-33.44
Fe(s)	0	0	0
Fe ₃ O ₄ (s)	-242.0091	-1012	-1013.73
Fe(OH) ₂ (s)	-116.3	-486.6	-491.96
FeCO ₃ (s)	-159.345	-666.7	-680.076
FeS ₂ (s)	-38.2956	-160.2	-156.17
FeS(am)	-	-	-95.17
FeS(s, troilite)	-	-	-101.954

7.2.1 Fe/H₂O System

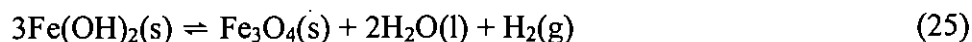
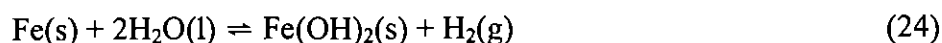
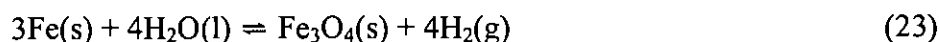
As explained by Brush (1990), two possible anoxic corrosion products of metallic Fe in the absence of CO₂ are Fe₃O₄ and (Fe,Mg)(OH)₂. Chivot (2004) selected the following solubilities for these materials:





Fe_3O_4 , which contains both ferric and ferrous species ($\text{Fe}(\text{II})\text{Fe}_2(\text{III})\text{O}_4$), is the stable Fe corrosion product encountered. It can be obtained by oxidation of $(\text{Fe},\text{Mg})(\text{OH})_2$, Fe oxidation by water vapor, or through the reduction of $\gamma\text{FeOOH}(\text{s})$. $\text{Fe}(\text{OH})_2(\text{s})$ is a pale green (crystalline) or white (amorphous) solid obtained by preparing a basic Fe solution in the total absence of O_2 .

Brush (1990) calculated the amount gas generated from the formation of $\text{Fe}_3\text{O}_4(\text{s})$ and $\text{Fe}(\text{OH})_2(\text{s})$ via the following equilibria:



The free energy of the chemical equilibria (23), (24), and (25) can be expressed as:

$$\Delta G_{23}^0 = -2.303 \times R \times T \times \log \left(\frac{\{\text{Fe}_3\text{O}_4(\text{s})\} \times f_{\text{H}_2}^4}{\{\text{Fe}(\text{s})\}^3 \times \{\text{H}_2\text{O}(\text{l})\}^4} \right) \quad (26)$$

$$\Delta G_{24}^0 = -2.303 \times R \times T \times \log \left(\frac{\{\text{Fe}(\text{OH})_2(\text{s})\} \times f_{\text{H}_2}}{\{\text{Fe}(\text{s})\} \times \{\text{H}_2\text{O}(\text{l})\}^2} \right) \quad (27)$$

$$\Delta G_{25}^0 = -2.303 \times R \times T \times \log \left(\frac{\{\text{Fe}_3\text{O}_4(\text{s})\} \times \{\text{H}_2\text{O}(\text{l})\}^2 \times f_{\text{H}_2}}{\{\text{Fe}(\text{OH})_2(\text{s})\}^3} \right) \quad (28)$$

Using $\{\text{Fe}_3\text{O}_4(\text{s})\} = \{\text{Fe}(\text{OH})_2(\text{s})\} = \{\text{Fe}(\text{s})\} = 1$, $\{\text{H}_2\text{O}(\text{l})\} = 0.7$, and Brush's selection of free energies presented in Table 2, the chemical equilibria (23) and (24), which describe the formations of $\text{Fe}_3\text{O}_4(\text{s})$ and $\text{Fe}(\text{OH})_2(\text{s})$ from the anoxic corrosion of $\text{Fe}(\text{s})$ by $\text{H}_2\text{O}(\text{l})$, H_2 fugacities of about 447 and 71 atm are obtained, respectively. However, the formation of $\text{Fe}_3\text{O}_4(\text{s})$ through conversion of $\text{Fe}(\text{OH})_2(\text{s})$ yields a much larger H_2 fugacity of 10^5 atm. The same calculations conducted with the free energies selected by Chivot (2004), presented in Table

¹ In a reducing environment

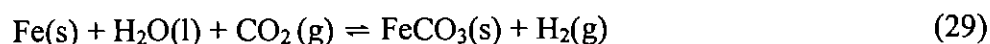
2 yield H₂ fugacities of 503, 616, and 273 atm, for the equilibria (23), (24), and (25), respectively.

The vast difference in the calculated fugacities for the equilibria involving Fe(OH)₂(s) (71 versus 616 atm, for Equation (27) and 10⁵ versus 273 atm, for Equation (28)) is due to the high sensitivity of the calculation to the value selected for the standard free energy of formation of Fe(OH)₂(s), $\Delta G_f^0(\text{Fe(OH)}_{2(s)})$. Brush selected the value of $\Delta G_f^0(\text{Fe(OH)}_{2(s)})$ from Wagman et al. (1969). However, Chivot had access to 10 data published between 1952 and 1999; he rejected four of them on a technical basis and calculated his selected value based on the Fe(OH)₂(s) standard enthalpy of formation, $\Delta H_f^0(\text{Fe(OH)}_{2(s)})$ and standard entropy, $\Delta S_f^0(\text{Fe(OH)}_{2(s)})$ published by Chase (1998). It is difficult at this point to favor one database over the other, as small variations in $\Delta G_f^0(\text{Fe(OH)}_{2(s)})$ have a large effect on the calculated H₂ fugacity. However, the $\Delta G_f^0(\text{Fe(OH)}_{2(s)})$ values published after 1990 are consistently smaller than the one published prior to 1990: the average is -493 ± 10 kJ/mol (or -490 ± 6 kJ/mol without the data rejected by Chivot) versus -484 ± 3 kJ/mol, which suggests that the data available in 1990 for $\Delta G_f^0(\text{Fe(OH)}_{2(s)})$ were slightly overestimated. Consequently, we favor the Chivot's database versus Brush's.

Chivot constructed the Pourbaix diagram for a Fe/H₂O system at 25° C, containing 10⁻⁶ m of dissolved Fe (Chivot, 2004, Figure 7). Under such conditions and at pH 9, FeOOH(s), Fe₃O₄, and Fe(s) are the solid stable phases for potentials (relative to the normal hydrogen electrode (NHE)) higher than $-0.35 V_{\text{NHE}}$, between -0.35 and $-0.50 V_{\text{NHE}}$, and lower than $-0.50 V_{\text{NHE}}$, respectively. The dissolved species are Fe(OH)₃⁰ and Fe(OH)₄⁻, for a positive potential and Fe²⁺ for a negative potential.

7.2.2 Fe/H₂O/CO₂ System

Microbes may produce CO₂(g), as illustrated by equations (7), (8), and (9). CO₂(g) can interact with Fe(s) to form FeCO₃(s). Brush (1990) describes the most likely corrosion reaction for this process as:



The dissociation reaction for FeCO₃ is described in Equation (30); the solubility product was selected by Chivot as:



The reaction pathway is the same whether Fe₃O₄(s) or Fe(OH)₂(s) is the intermediate product. The free energy of the chemical equilibrium (29) can be expressed as:

$$\Delta G_{29}^0 = -R \times T \times \ln(10) \times \log \left(\frac{\{FeCO_3(s)\} \times f_{H_2}}{\{Fe(s)\} \times \{H_2O(l)\} \times f_{CO_2}} \right) \quad (31)$$

Using $\{FeCO_3(s)\} = \{Fe(s)\} = 1$, $\{H_2O(l)\} = 0.7$, and Brush's selection of free energies (see Table 2), the chemical equilibrium (29) yields a ratio of fugacities, $\log \frac{f_{H_2}}{f_{CO_2}}$, of 6.01.

With Chivot's selection of free energy values, this ratio increases 8.36. In both cases, the value indicates that the $H_2(g)$ fugacity will exceed that of $CO_2(g)$.

Chivot has calculated the Pourbaix diagram for a Fe/ H_2O / CO_2 system at 25 °C, containing 10^{-6} m of dissolved Fe and several dissolved carbon concentrations: 10^{-4} , 10^{-3} , and 10^{-2} m (Chivot, 2005, Figures 11-12). Total dissolved carbon concentrations of 10^{-4} , 10^{-3} , and 10^{-2} m are in equilibrium with $CO_2(g)$ fugacities of $10^{-5.2}$, $10^{-4.2}$, and $10^{-3.2}$ atm, respectively, at pH 9. These fugacities were calculated using Chivot's values for the $CO_2(g)/CO_2^0/HCO_3^-/CO_3^{2-}$ system:



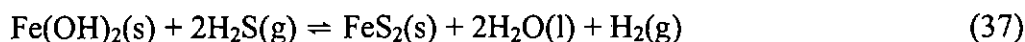
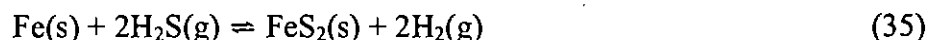
With: $\log \alpha = \log \frac{\{CO_2^0\}}{P_{CO_2}} = -1.47$, $\log K_{33} = \log \left(\frac{\{HCO_3^-\} \times \{H^+\}}{\{CO_2^0\}} \right) = -6.35$, and

$$\log K_{34} = \log \left(\frac{\{CO_3^{2-}\} \times \{H^+\}}{\{HCO_3^-\}} \right) = -10.33$$

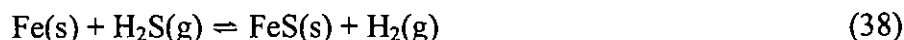
An increase of total dissolved carbon concentrations from 10^{-4} to 10^{-2} m leads to a substantially larger region of stability for $FeCO_3$. At pH 9, $FeCO_3$ occurs at potentials between -0.61 and -0.52 V_{NHE} , for a $P_{CO_2(g)}$ of $10^{-5.2}$ atm, and at potentials between -0.67 and -0.37 V_{NHE} , for a $P_{CO_2(g)}$ of $10^{-3.2}$ atm.

7.2.3 Fe/ H_2O / H_2S System

Microbes may reduce sulfate (SO_4^{2-}) to produce $H_2S(aq$ or $g)$, as shown in Equation (8). $H_2S(g)$ interaction with $Fe(s)$ may produce a number of solids, including $(Fe,Ni)S(s)$, $FeS_{1-x}(s)$ (with $x = 0$ to 0.2), $FeS(s)$, $FeS \cdot nH_2O(s)$, $Fe_3S_4(s)$, and $FeS_2(s)$. The formation $FeS_2(s)$ can be described by the following equilibria (Equations (35) to (37)):



However, the WIPP PA considers only the formation of FeS(s), the sole iron sulfide specie observed by Telander and Westerman (1997) in WIPP brines. FeS(s) formation can be described by the following equilibrium:



The solubility product of FeS(s) defined as Equation (39) was selected by Chivot (2004) as:



The free energy of the chemical equilibrium (38) can be expressed as:

$$\Delta G_{38}^0 = -R \times T \times \ln(10) \times \log \left(\frac{\{\text{FeS(s)}\} \times f_{\text{H}_2}}{\{\text{Fe(s)}\} \times f_{\text{H}_2\text{S}}} \right) \quad (40)$$

Using $\{\text{FeS(s)}\} = \{\text{Fe(s)}\} = 1$ and Chivot's (2004) selection of free energies for H₂S(g) and amorphous FeS(s) (see Table 2), the ratio of gas fugacities, $\log \frac{f_{\text{H}_2}}{f_{\text{H}_2\text{S}}}$, is 10.80. This indicates that the H₂(g) fugacity will exceed that of H₂S(g).

Chivot constructed the Pourbaix diagram for a Fe/H₂O/H₂S system at 25 °C, containing 10⁻⁶ m of dissolved Fe and several dissolved carbon concentrations: 10⁻⁴, 10⁻³, and 10⁻² m, for the solid and dissolved species, respectively. Total dissolved sulfur concentrations of 10⁻⁴, 10⁻³, and 10⁻² m are in equilibrium with H₂S(g) fugacities of 10^{-5.0}, 10⁻⁴, and 10^{-3.0} atm, respectively, at pH 9. These fugacities are calculated using Chivot's (2004) values for the H₂S(g)/H₂S⁰/HS⁻/S²⁻ system:



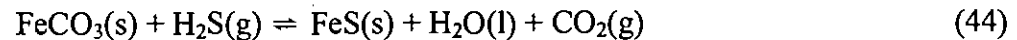
$$\text{With: } \log \alpha = \log \frac{\{H_2S^0\}}{P_{H_2S(g)}} = -1.02, \log K_{42} = \log \left(\frac{\{HS^-\} \times \{H^+\}}{\{H_2S^0\}} \right) = -6.99, \text{ and}$$

$$\log K_{43} = \log \left(\frac{\{S^{2-}\} \times \{H^+\}}{\{HS^-\}} \right) = -17.10$$

An increase of the total dissolved sulfur concentrations from 10^{-4} to 10^{-2} m expands the region of stability of the solid iron sulfides. At 10^{-4} m, $FeS_2(s)$ is stable from pH 1.2 to 11.7 and $FeS(s)$ from pH 6 to 11, but at 10^{-3} m, the stability region of $FeS_2(s)$ ranges from pH 0.5 to 13.5 and $FeS(s)$ from pH 5 to 14.5. At pH 9, $FeS_2(s)$ can be found between -0.43 and -0.26 V at 10^{-4} m $H_2S(g)$ and between -0.54 and -0.29 V_{NHE} at 10^{-2} m $H_2S(g)$; $FeS(s)$ can be found between -0.7 and -0.43 V_{NHE} at 10^{-4} m $H_2S(g)$ and between -0.77 and -0.54 V_{NHE} at 10^{-2} m $H_2S(g)$. As for the dissolved species, an increase of the total dissolved sulfur concentrations from 10^{-4} to 10^{-2} m leads to an increase of the stability region of $FeSO_4^+$, the disappearance for $FeOH^{2+}$, and the appearance of $FeSO_4^0$, which replaces part of the stability region of Fe^{2+} .

7.2.4 Fe/H₂O/CO₂/H₂S System

In the presence of both $CO_2(g)$ and $H_2S(g)$, the resulting $FeCO_3$, formed from the interaction of $Fe(s)$ and $CO_2(g)$, reacts with $H_2S(g)$ to form $FeS(s)$:



The free energy of the chemical equilibria (44) can be expressed as:

$$\Delta G_{44}^0 = -R \times T \times \ln(10) \times \log \left(\frac{\{FeS(s)\} \times \{H_2O\} \times f_{CO_2}}{\{FeCO_3(s)\} \times f_{H_2S}} \right) \quad (45)$$

Using $\{FeS(s)\} = \{FeCO_3(s)\} = 1$ and $\{H_2O(l)\} = 0.7$, and Chivot's selection of free energies presented in Table 2, the chemical equilibria (44) leads to the ratio of gas fugacities, $\log \frac{f_{CO_2}}{f_{H_2S}} = 2.44$. Therefore, the $CO_2(g)$ produced always exceeds the amount of $H_2S(g)$ consumed by the process. Moreover, laboratory and modeling studies have shown that the carbonation reaction of the MgO engineered barrier will buffer f_{CO_2} at a value of $10^{-5.50}$ atm in WIPP brines (see Section 7.2). Therefore, the fugacity of $H_2S(g)$ resulting from the formation of $FeS(s)$ in the WIPP is predicted to be $10^{-6.9}$ atm.

The instability of $FeCO_3$ in the presence of $H_2S(g)$ has been illustrated with several diagrams. Garrels and Christ published a Pourbaix diagram for the system $Fe/H_2O/CO_2/H_2S$ (Garrels and Christ, 1990, Figure 7.23), merely a superposition of the diagrams they calculated for the systems $Fe/H_2O/CO_2$ and $Fe/H_2O/H_2S$. A system containing total dissolved concentrations of 10^{-4} M for S and 1 M for the carbonate (i.e. $f_{H_2S} = 10^{-5}$ atm and $f_{CO_2} = 10^{-1.2}$ atm, at pH 9) shows that Fe oxides ($Fe_2O_3(s)$, $Fe_3O_4(s)$), carbonate ($FeCO_3(s)$), and sulfide ($FeS_2(s)$) are stable.

FeS(s), however, has totally disappeared, its stability region replaced by that of FeCO₃(s). This contradicts Equation (44), where the free energy ΔG^0 is negative, indicating that the reaction is spontaneous as written. This is clearly an artifact of the superposition of the Fe/H₂O/CO₂ and Fe/H₂O/H₂S diagrams, which does not account for the equilibrium described in Equation (44). Garrels and Christ demonstrated that with lower and more realistic f_{CO_2} (e.g. $10^{-3.2}$ atm, at pH 9), only Fe oxides and sulfide (FeS₂(s)) are stable and that FeCO₃ completely disappears from the diagram. This observation is particularly evident in Figure 6.10 of Garrels and Christ's publication (1990), which shows a partial pressure diagram of the system Fe/O₂/CO₂/S₂. FeCO₃(s) is the stable specie for relatively high f_{CO_2} . In quasi-total absence of O₂(g) (10^{-100} atm), FeCO₃ is stable for f_{CO_2} greater than $10^{1.4}$ atm. However, with an infinitesimally larger f_{O_2} (10^{-88} - 10^{-68} atm), FeCO₃ occurs at f_{CO_2} as low as $10^{-4.5}$ atm.

7.3 Pb Systems

Metallic Pb is oxidized in water, at 25 °C and 1 atm, though at lower rates than Fe. This oxidation process results in a number of species, as detailed below.

In the following text, thermodynamic calculations are performed which result in an estimated quantity of gas generated by the corrosion of Pb by H₂O, CO₂, and H₂S. The standard free energies utilized in these calculations are presented in Table 3.

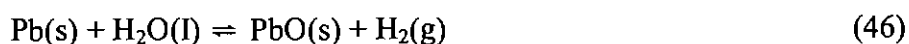
Table 3. Free Energies Selected by the USGS (1995) and Chivot (2004).

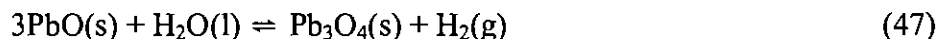
Compound	ΔG_f^0 selected by USGS (1995) (kJ/mol)	ΔG_f^0 selected by Chivot (2004) (kJ/mol)
H ₂ O(l)		-237.140
H ₂ (g)		0
H ⁺		0
CO ₂ (g)		-394.373
H ₂ S(g)		-33.44
Pb(s)	0	
PbO(s) litharge	-188.9	
PbO(s) massicot	-187.9	
Pb ₃ O ₄ (s)	-601.6	
PbCO ₃ (s)	-625.5	
PbS(s)	-96.8	

7.3.1 Pb/H₂O System

Metallic Pb will oxidize in water to form a number of species, including PbO(s), Pb₃O₄(s), Pb₂O₃(s), and PbO₂(s). Pb(OH)₂(s) is also a Pb(II) solid, but no evidence of its formation from metallic Pb could be found in the literature. The species likely to occur in an anoxic environment are PbO(s) and Pb₃O₄(s); both of which are soluble in acid. However, metallic Pb is thermodynamically stable in the presence of neutral or alkaline aqueous solutions in an anoxic environment, as a portion of its stability domain is located above the H₂/H₂O line of the Pourbaix diagram, as illustrated in by Pourbaix (1974, p. 489 Figure 1).

The formation of PbO(s) and Pb₃O₄(s) in an anoxic environment is described in equations (46) and (47).





The free energy of the chemical equilibria (46) and (47) can be expressed as:

$$\Delta G_{46}^0 = -R \times T \times \ln(10) \times \log \left(\frac{\{\text{PbO(s)}\} \times f_{\text{H}_2}}{\{\text{Pb(s)}\} \times \{\text{H}_2\text{O(l)}\}} \right) \quad (48)$$

$$\Delta G_{47}^0 = -R \times T \times \ln(10) \times \log \left(\frac{\{\text{Pb}_3\text{O}_4\text{(s)}\} \times f_{\text{H}_2}}{\{\text{PbO(s)}\}^3 \times \{\text{H}_2\text{O(l)}\}} \right) \quad (49)$$

Using $\{\text{Pb}_3\text{O}_4\text{(s)}\} = \{\text{PbO(s)}\} = \{\text{Pb(s)}\} = 1$, $\{\text{H}_2\text{O(l)}\} = 0.7$, and the free energies presented in Table 3, the chemical equilibria (46) and (47), which describe the formations of PbO(s) and $\text{Pb}_3\text{O}_4\text{(s)}$ from the anoxic corrosion of Pb(s) and PbO(s) by $\text{H}_2\text{O(l)}$, yield H_2 fugacities of approximately 10^{-9} and 10^{-36} atm, respectively.

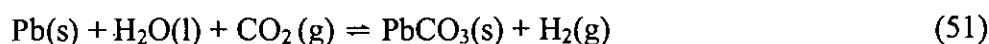
A E_h -pH diagram for the $\text{Pb}/\text{H}_2\text{O}$ system at 25°C was produced by Pourbaix (1974, p.489 Figure 1). It shows the stability regions of the Pb solid and dissolved species for different Pb concentrations and $\text{PbH}_2\text{(g)}$ pressures. At pH 9, with 1 M Pb , and 1 atm $P_{\text{PbH}_2\text{(g)}}$, Pb(s) , PbO(s) , $\text{Pb}_3\text{O}_4\text{(s)}$, and $\text{PbO}_2\text{(s)}$ are the solid stable phases for potentials between -0.2 than $-0.3 V_{\text{NHE}}$, between -0.3 and $0.4 V_{\text{NHE}}$, between 0.4 and $0.6 V_{\text{NHE}}$, and above $0.6 V_{\text{NHE}}$, respectively.

7.3.2 $\text{Pb}/\text{H}_2\text{O}/\text{CO}_2$ System

Pb(s) reacts with $\text{CO}_2\text{(g)}$ to form $\text{PbCO}_3\text{(s)}$, cerussite. The solubility product of this solid is obtained from Lide (2004-2005):



The formation of $\text{PbCO}_3\text{(s)}$ is described in Equation (51):



The free energy of the reaction shown in Equation (51) can be expressed as:

$$\Delta G_{51}^0 = -R \times T \times \ln(10) \times \log \left(\frac{\{\text{PbCO}_3\text{(s)}\} \times f_{\text{H}_2}}{\{\text{Pb(s)}\} \times \{\text{H}_2\text{O(l)}\} \times f_{\text{CO}_2}} \right) \quad (52)$$

Using $\{PbCO_3(s)\} = \{Pb(s)\} = 1$, $\{H_2O(l)\} = 0.7$, and the selection of free energies presented in Table 3, the chemical equilibrium (52) leads to a ratio of fugacities $\log \frac{f_{H_2}}{f_{CO_2}}$ of -1.21, which indicates that $CO_2(g)$ fugacity would slightly exceed that of $H_2(g)$.

Garrels and Christ (1990) produced Pourbaix diagrams for the system $Pb/H_2O/CO_2$, for CO_2 fugacities of 10^{-4} and $10^{-2.7}$ atm (Garrels and Christ, 1990, Figures 7.26a and 7.26b). An increase in $CO_2(g)$ pressure from 10^{-4} to $10^{-2.7}$ atm leads to the formation of $Pb_3(OH)_2(CO_3)_2(s)$, $Pb_3O_4(s)$ and PbO . The increase in $CO_2(g)$ also reduces the E_h at which metallic Pb is stable. At pH 9 and $f_{CO_2} = 10^{-4}$ atm, $Pb(s)$, $PbCO_3(s)$, and $PbO_2(s)$ are stable for E_h lower than $-0.37 V_{NHE}$, between -0.37 and $+0.63 V_{NHE}$, and higher than $+0.63 V_{NHE}$, respectively.

7.3.3 Pb/H₂O/H₂S System

$Pb(s)$ reacts with $H_2S(g)$ to form $PbS(s)$. The solubility product of this solid is obtained from Lide (2004-2005):



The formation of $PbS(s)$ is described by Equation (54):



The free energy of the chemical equilibrium (54) can be expressed as:

$$\Delta G_{54}^0 = -R \times T \times \ln(10) \times \log \left(\frac{\{PbS(s)\} \times f_{H_2}}{\{Pb(s)\} \times f_{H_2S}} \right) \quad (55)$$

Using $\{PbS(s)\} = \{Pb(s)\} = 1$ and the selection of free energies presented in Table 3, the ratio of gas fugacities, $\log \frac{f_{H_2}}{f_{H_2S}}$ is 11.11. This implies that $H_2(g)$ fugacity would exceed that of $H_2S(g)$.

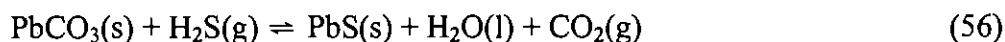
Garrels and Christ produced a Pourbaix diagram for the system $Pb/H_2O/CO_2$ (Garrels and Christ, 1990, Figure 7.26c). Even at a total S of only 10^{-5} m, (i.e., 10^{-6} atm $H_2S(g)$, at pH 9), both $PbSO_4(s)$ and $PbS(s)$ have large stability fields and the region of stability for metallic Pb is pushed to substantially lower E_h . At pH 9, $PbS(s)$, $PbSO_4(s)$, and $PbO_2(s)$ are the only thermodynamically stable species; they occur for E_h below $-0.26 V_{NHE}$, between -0.26 and $+0.5 V_{NHE}$, and above $+0.5 V_{NHE}$, respectively.

7.3.4 Pb/H₂O/CO₂/H₂S System

Garrels and Christ's produced a Pourbaix diagram for the system $Pb/H_2O/CO_2/H_2S$ (1990, Figure 7.26e). This diagram pertains to relatively high sulfur and carbonate

concentrations: $10^{-1.5}$ m (i.e., $f_{\text{H}_2\text{S}} = 10^{-2.5}$ atm, at pH 9) and 10^{-1} m (i.e., $f_{\text{CO}_2} = 10^{-2.2}$ atm, at pH 9), respectively. At such f_{CO_2} , $\text{Pb}_3(\text{OH})_2(\text{CO}_3)_2(\text{s})$, $\text{Pb}_3\text{O}_4(\text{s})$, and $\text{PbO}(\text{s})$ are stable within the pH and E_h boundaries described in this diagram; however, these solids do not appear at more relevant f_{CO_2} levels (e.g., 10^{-4} atm) where the region of stability for $\text{PbCO}_3(\text{s})$ extends to pH 13, above which the soluble HPbO_2^- is stable. The inclusion of $10^{-1.5}$ m of sulfur in the $\text{Pb}/\text{H}_2\text{O}/\text{CO}_2$ system leads to the appearance of PbS , a small region where PbS and S are both stable, and the reduction of the region of stability for metallic Pb to very low values of E_h and high pH. Unlike Fe , for which the stability region of the sulfide minerals replaces that of the carbonates, the Pb sulfide material only reduces the stability regions of the carbonates. This is illustrated in a partial pressure diagram published by Garrels and Christ's, for the system $\text{Pb}/\text{H}_2\text{O}/\text{CO}_2/\text{S}$ (1990, Figure 6.17). $\text{PbCO}_3(\text{s})$ can form at CO_2 pressures as low as 10^{-5} atm, a value far below the $10^{1.4}$ atm required for the stability of FeCO_3 . At pH 9 and in the conditions described by 7.26e of Garrels and Christ (1990), the stable solids are $\text{PbS}(\text{s})$, $\text{PbCO}_3(\text{s})$, and $\text{PbO}_2(\text{s})$, for potentials below $-0.27 V_{\text{NHE}}$, between -0.27 and $+0.67 V_{\text{NHE}}$, and greater than $+0.67 V_{\text{NHE}}$, respectively.

Based upon the two figures discussed above (Garrels and Christ, 1990, Figures 7.26e and 6.17), we anticipate that $\text{PbCO}_3(\text{s})$ will interact with $\text{H}_2\text{S}(\text{g})$, in a similar fashion as iron carbonate does:



The free energy of the chemical equilibria (56) can be expressed as:

$$\Delta G_{56}^0 = -R \times T \times \ln(10) \times \log \left(\frac{\{\text{PbS}(\text{s})\} \times \{\text{H}_2\text{O}(\text{l})\} \times f_{\text{CO}_2}}{\{\text{PbCO}_3(\text{s})\} \times f_{\text{H}_2\text{S}}} \right) \quad (57)$$

Using $\{\text{PbS}(\text{s})\} = \{\text{PbCO}_3(\text{s})\} = 1$ and $\{\text{H}_2\text{O}(\text{l})\} = 0.7$, and Chivot's selection of free energies presented in Table 3, the chemical equilibrium (57) leads to the ratio of gas fugacities, $\log \frac{f_{\text{CO}_2}}{f_{\text{H}_2\text{S}}} = 12.32$. Therefore, the $\text{CO}_2(\text{g})$ produced exceeds the amount of $\text{H}_2\text{S}(\text{g})$ consumed by the process. The fugacity of $\text{CO}_2(\text{g})$ in the WIPP brine is predicted to equilibrate at $10^{-5.50}$ atm (see Section 5.2), therefore, the fugacity of $\text{H}_2\text{S}(\text{g})$ resulting from the formation of $\text{PbS}(\text{s})$ in the WIPP is predicted to be $10^{-17.8}$ atm.

7.4 Summary of the Thermodynamic Calculations

In an $\text{Fe}/\text{H}_2\text{O}$ system, the formation of $\text{Fe}_3\text{O}_4(\text{s})$ or $\text{Fe}(\text{OH})_2(\text{s})$ from the oxidation of $\text{Fe}(\text{s})$, and the formation of $\text{Fe}_3\text{O}_4(\text{s})$ from the decomposition of $\text{Fe}(\text{OH})_2(\text{s})$ produce large quantities of $\text{H}_2(\text{g})$ (the resulting $f_{\text{H}_2(\text{g})}$ are 503, 616, and 273 atm, respectively). In an $\text{Pb}/\text{H}_2\text{O}$ system, the formations of the Pb solids generates much less $\text{H}_2(\text{g})$ than Fe does in similar conditions; the formations of $\text{PbO}(\text{s})$ and $\text{Pb}_3\text{O}_4(\text{s})$ yield $\text{H}_2(\text{g})$ fugacities of 10^{-9} and 10^{-36} atm, respectively. In reducing environment and at pH 9, the stable Fe solid species are $\text{FeOOH}(\text{s})$, $\text{Fe}_3\text{O}_4(\text{s})$, and $\text{Fe}(\text{s})$, stable in a system containing 10^{-6} m dissolved Fe for E_h higher than

$-0.35 V_{\text{NHE}}$, between -0.35 and $-0.50 V_{\text{NHE}}$, and lower than $-0.50 V_{\text{NHE}}$, respectively. $\text{Fe}(\text{OH})_{2(\text{s})}$ is not stable at pH 9 in pure water. In reducing environment and at pH 9, $\text{PbO}(\text{s})$ and $\text{Pb}(\text{s})$ are the stable solid species, occurring for potentials between -0.3 and $0.4 V_{\text{NHE}}$, and below $-0.3 V_{\text{NHE}}$, respectively, for a system containing 1 M total Pb. In those conditions, $\text{Pb}_3\text{O}_4(\text{s})$ is stable for E_{h} values between 0.4 and $0.6 V_{\text{NHE}}$.

In an $\text{Fe}/\text{H}_2\text{O}/\text{CO}_2$ system, the formation of $\text{FeCO}_3(\text{s})$ yields a ratio of the fugacities between $\text{H}_2(\text{g})$ and $\text{CO}_2(\text{g})$ equal to $10^{8.36}$. However, the stability region of $\text{FeCO}_3(\text{s})$ is very small. For example, in a system at pH 9, containing 10^{-6} m dissolved Fe, and with a $\text{CO}_2(\text{g})$ fugacity of $10^{-5.2}$ atm (close to that set by the brucite-hydromagnesite buffer, $10^{-5.5}$ atm), FeCO_3 occurs at potentials between -0.61 and $-0.52 V_{\text{NHE}}$. The stability region becomes larger with increasing $f_{\text{CO}_2(\text{g})}$. In an $\text{Pb}/\text{H}_2\text{O}/\text{CO}_2$ system, the formation of $\text{PbCO}_3(\text{s})$ yields a ratio of fugacities between $\text{H}_2(\text{g})$ and $\text{CO}_2(\text{g})$ equal to $10^{1.21}$, smaller than that for the Fe system. But the stability region of $\text{PbCO}_3(\text{s})$ is much larger than that of $\text{FeCO}_3(\text{s})$; at pH 9 and $f_{\text{CO}_2} = 10^{-4}$ atm, $\text{PbCO}_3(\text{s})$ is stable for E_{h} ranging from -0.37 to $+0.63 V_{\text{NHE}}$.

Out of all the solid iron sulfide species, the WIPP PA considers only $\text{FeS}(\text{s})$, which formation yields a ratio of gas fugacities between $\text{H}_2(\text{g})$ and $\text{H}_2\text{S}(\text{g})$ of $10^{10.80}$, for an $\text{Fe}/\text{H}_2\text{O}/\text{H}_2\text{S}/$ system. If such a system contains 10^{-4} m $\text{H}_2\text{S}(\text{g})$, $\text{FeS}(\text{s})$ can be found between -0.7 and $-0.43 V_{\text{NHE}}$. An increase of $\text{H}_2\text{S}(\text{g})$ only increases the stability region of $\text{FeS}(\text{s})$ to higher pH values. In a $\text{Pb}/\text{H}_2\text{O}/\text{H}_2\text{S}$ system, the formation of $\text{PbS}(\text{s})$ formation yields a ratio of gas fugacities between $\text{H}_2(\text{g})$ and $\text{H}_2\text{S}(\text{g})$ of $10^{11.11}$, quite similar to that for the Fe system. $\text{PbS}(\text{s})$ is stable for higher Eh than $\text{FeS}(\text{s})$ is. At pH 9, $\text{PbS}(\text{s})$ is the thermodynamically stable species for E_{h} below $-0.26 V_{\text{NHE}}$.

In a system containing both $\text{H}_2\text{S}(\text{g})$ and $\text{CO}_2(\text{g})$, $\text{FeCO}_3(\text{s})$ is unstable, as $\text{FeS}(\text{s})$ can form from the sulfidization of $\text{FeCO}_3(\text{s})$. This reaction produces slightly more $\text{CO}_2(\text{g})$ than $\text{H}_2\text{S}(\text{g})$ is consumed by the process; for example, for a $10^{-5.5}$ atm $\text{CO}_2(\text{g})$ fugacity, the fugacity of the produced $\text{H}_2\text{S}(\text{g})$ is $10^{-6.9}$ atm. This $\text{H}_2\text{S}(\text{g})$ fugacity is much lower ($10^{-17.8}$ atm) for the formation of $\text{PbS}(\text{s})$ in similar conditions. $\text{FeCO}_3(\text{s})$ is very unstable in presence of sulfide; in quasi-total absence of $\text{O}_2(\text{g})$ (10^{-100} atm), FeCO_3 is only stable for f_{CO_2} greater than $10^{1.4}$ atm. But $\text{PbCO}_3(\text{s})$ can form at CO_2 pressures as low as 10^{-5} atm, a value far below that required for the stability of $\text{FeCO}_3(\text{s})$.

7.5 Calculations Involving Microbial Gas Generation

The total volume of waste to be emplaced in the WIPP is $175,564 \text{ m}^3$, with CH and RH waste volumes of $1.69 \times 10^5 \text{ m}^3$ and $7,080 \text{ m}^3$, respectively (US Congress, 1992). The total quantity of C from the CPR is 1.10×10^9 mol (Nemer and Stein, 2005), the total quantity of NO_3 and SO_4^{2-} from the waste are 4.31×10^7 and 4.61×10^6 mol, respectively, as recorded in the WIPP parameter database (WIPP PA, 2001a; WIPP PA, 2001b). The following sections detail the impact which Fe and Pb could potentially have on the microbial gasses, with a clear focus on the consumption of CO_2 via the formation of metal carbonates. In order to simplify these calculations, it was assumed that all of the material (Fe or Pb) was available for consumption. As such, the values presented below represent the upper limit of CO_2 consumption and carbonate formation by the Fe and Pb present within WIPP.

7.5.1 Impact of Fe on Microbial Gases

Crawford (Crawford, 2005a) published the values for the disposal inventory for Fe-base metals and alloys; for the purpose of the following calculations, we consider the Fe-base metals and alloys (e.g. steel) to be 100 % Fe. The estimated Fe densities are 110 and 59 kg/m³, in the CH and RH waste, and 170 and 540 kg/m³, in the CH and RH waste containers, at closure time. Therefore, considering CH and RH volumes of 1.69×10^5 and 7,080 m³, respectively (U.S. Congress, 1992), the estimated Fe mass in the CH and RH wastes, including the containers, is 4.7×10^7 and 4.2×10^6 kg, respectively, which total to 9.2×10^8 mol of Fe in WIPP, or 1,094 mol Fe per equivalent drum. Lappin (1989) had estimated this number at 900 mol Fe per drum equivalent.

7.5.1.1 DENITRIFICATION, SULFATE REDUCTION, NO METHANOGENESIS

The WIPP PA simulations assume that microbial gas generation may occur only through a combination of denitrification and sulfate reduction (Equations (7) and (8)), as specified by the EPA (Cotsworth, 2004, Comment G-14). During denitrification (Equation (7)), microbes consume 6 mol of C and 4.8 mol of NO₃⁻ and produce 6 mol of CO₂(g) and 2.4 mol of N₂(g). Therefore, if all of the NO₃⁻ contained within the inventory were consumed, the total quantity of CPR C consumed would be:

$$4.31 \times 10^7 \times \frac{6}{4.8} = 5.39 \times 10^7 \text{ moles C} \quad (58)$$

Similarly, the quantities of CO₂(g) and N₂(g) generated by the denitrification process are 5.39×10^7 and 2.16×10^7 mol, respectively. During sulfate reduction (Equation (8)), 6 mol of C react with 3 mol of SO₄²⁻ to produce 6 mol of CO₂(g) and 3 mol of H₂S(g). Although the inventory contains 4.61×10^6 mol of SO₄²⁻, additional sulfate may be available from the WIPP structure itself (i.e., from marker beds, brines), and as such it is difficult to quantify exactly how much sulfate is available for microbial activity. The EPA has required that we assume that sufficient SO₄²⁻ is available to consume all remaining C (after denitrification) in CPR materials. The total quantity of carbon consumed by the sulfate reduction process is the difference between the total C available from the CPR (1.10×10^9) and the total quantity of C consumed by the denitrification process (5.39×10^7), which is 1.05×10^9 mol of C. The amount of H₂S(g) and CO₂(g) produced by sulfate reduction is 5.24×10^8 and 1.05×10^9 mol, respectively. As a result, if all of the carbon available within the WIPP CPR is consumed by sulfate reduction, the resulting quantity of CO₂(g) would be the sum of that produced by each of the aforementioned processes, or 1.10×10^9 mol.

Section 7.2.2 demonstrated that the fugacity of H₂(g) produced by the formation of FeCO₃ exceeds that of CO₂(g) consumed during the process by 8 orders of magnitude. Therefore, if sufficient Fe(s) was available, nearly all the CO₂(g) generated by the microbial activity would be consumed during FeCO₃ formation. The production of FeCO₃ from 1.10×10^9 mol CO₂(g) (Equation (29)) would consume 1.10×10^9 mol Fe(s), which exceeds the total Fe inventory (9.2×10^8 Fe mol). Therefore, if the total Fe inventory is consumed by the production of FeCO₃, only 9.2×10^8 mol CO₂(g) will be consumed, 9.2×10^8 mol of FeCO₃(s)

will be produced, and 1.8×10^8 mol $\text{CO}_2(\text{g})$ (16% of the total predicted quantity of $\text{CO}_2(\text{g})$) will remain unreacted.

Section 7.2.4 demonstrated that the fugacity of $\text{CO}_2(\text{g})$ produced during the formation of $\text{FeS}(\text{s})$, as described by Equation (44), exceeds that of $\text{H}_2\text{S}(\text{g})$ consumed during this process by over 2 orders of magnitude. Calculations presented above determined that the sulfate reduction reaction produced 5.24×10^8 mol of $\text{H}_2\text{S}(\text{g})$. However, 9.2×10^8 mol of $\text{FeCO}_3(\text{s})$ are formed. Thus the limiting reagent for the formation of $\text{FeS}(\text{s})$ is $\text{H}_2\text{S}(\text{g})$. As such, the reaction between $\text{H}_2\text{S}(\text{g})$ and $\text{FeCO}_3(\text{s})$ will generate 5.24×10^8 mol of $\text{CO}_2(\text{g})$ and leave 4.0×10^8 mol of $\text{FeCO}_3(\text{s})$ unreacted.

The total quantity of $\text{CO}_2(\text{g})$ remaining after the production of $\text{FeCO}_3(\text{s})$ and $\text{FeS}(\text{s})$ is 7.0×10^8 mol, which is then available to react with the engineered barrier MgO to form $\text{Mg}_5(\text{CO}_3)_4(\text{OH})_2 \cdot 4\text{H}_2\text{O}$. Table 4 summarizes the results of the previous series of calculations.

Table 4. Result Summaries for Fe-Gas Reactions With the Denitrification And Sulfate Reduction Processes, but Without Methanogenesis.

Material available (mol)	Reactants (mol)	Products (mol)	Unreacted Materials (mol)
$C_6H_{10}O_5 + 4.8H^+ + 4.8NO_3^- \rightarrow 7.4H_2O(l) + 6CO_2(g) + 2.4N_2(g)$			
C: 1.10×10^9 NO ₃ ⁻ : 4.31×10^7	C: 5.39×10^7 NO ₃ ⁻ : 4.31×10^7	CO ₂ (g): 5.39×10^7 N ₂ (g): 2.16×10^7	C: 1.05×10^9 NO ₃ ⁻ : 0
$C_6H_{10}O_5 + 6H^+ + 3SO_4^{2-} \rightarrow 5H_2O(l) + 6CO_2(g) + 3H_2S(g)$			
C: 1.05×10^9 SO ₄ ²⁻ : unknown	C: 1.05×10^9 SO ₄ ²⁻ : 1.05×10^9	CO ₂ (g): 1.05×10^9 H ₂ S(g): 5.24×10^8	C: 0 SO ₄ ²⁻ : unknown
$Fe(s) + H_2O(l) + CO_2(g) = FeCO_3(s) + H_2(g)$			
Fe: 9.2×10^8 CO ₂ (g): 1.10×10^9	Fe: 9.2×10^8 CO ₂ (g): 9.2×10^8	FeCO ₃ (s): 9.2×10^8 H ₂ (g): 9.2×10^8	Fe: 0 CO ₂ (g): 1.8×10^8
$FeCO_3(s) + H_2S(g) = FeS(s) + H_2O(l) + CO_2(g)$			
FeCO ₃ (s): 9.2×10^8 H ₂ S(g): 5.24×10^8	FeCO ₃ (s): 5.24×10^8 H ₂ S(g): 5.24×10^8	FeS(s): 5.24×10^8 CO ₂ (g): 5.24×10^8	FeCO ₃ (s): 4.0×10^8 H ₂ S(g): 0

7.5.1.2 DENITRIFICATION, SULFATE REDUCTION, AND METHANOGENESIS

The calculations in this section include the methanogenesis process. Two cases have been considered here. In the first case, we consider that the sulfate available from both the waste and the WIPP rooms, which includes sulfate contained in marker beds and brines, will react with CPR carbon during sulfate reduction. In this case, the total quantity of sulfate available for reaction is unknown. In the second case, only the sulfate contributed by the waste emplaced within the WIPP is considered.

Case 1: 50% of the CPR Carbon Remaining After Denitrification Reacts With Sulfate and 50% Reacts With Water to Form CH₄

Calculations similar to those presented above were conducted with the assumption that half of the remaining unreacted CPR carbon following denitrification (i.e. 5.24×10^8 mol) will react through the sulfate reduction process and the other half through methanogenesis. Denitrification produces 5.39×10^7 mol of CO₂(g) and 2.16×10^7 mol of N₂(g) and leaves 1.05×10^9 mol of CPR carbon unreacted. Sulfate reduction will produce 5.24×10^8 mol of CO₂(g) and 2.62×10^8 mol H₂S(g) and methanogenesis will produce 2.62×10^8 mol of each CH₄(g) and CO₂(g). A total of 8.39×10^8 mol of CO₂(g) can then react with metallic Fe to form 8.39×10^8 mol of each FeCO₃(s) and H₂(g), leaving 8.4×10^7 mol of Fe(s) unreacted. The reaction between FeCO₃(s) and H₂S(s) produces 2.62×10^8 mol of each FeS(s) and CO₂(g). This newly generated CO₂(g) can then react with the unreacted Fe(s) to form an additional 8.4×10^7 mol of FeCO₃(s), leaving 1.8×10^8 mol of CO₂(g) unreacted. This remaining CO₂(g) can interact with the engineered barrier as described previously. This calculation is summarized in Table 5.

Table 5. Summary of the Results for Fe-Gas Reactions With Denitrification, Sulfate Reduction, and Methanogenesis Processes, Case 1.

Material available (mol)	Reactants (mol)	Products (mol)	Unreacted Materials (mol)
$C_6H_{10}O_5 + 4.8H^+ + 4.8NO_3^- \rightarrow 7.4H_2O(l) + 6CO_2(g) + 2.4N_2(g)$			
C: 1.10×10^9 NO ₃ ⁻ : 4.31×10^7	C: 5.39×10^7 NO ₃ ⁻ : 4.31×10^7	CO ₂ (g): 5.39×10^7 N ₂ (g): 2.16×10^7	C: 1.05×10^9 NO ₃ ⁻ : 0
$C_6H_{10}O_5 + 6H^+ + 3SO_4^{2-} \rightarrow 5H_2O(l) + 6CO_2(g) + 3H_2S(g)$			
C: 5.24×10^8 SO ₄ ²⁻ : unknown	C: 5.24×10^8 SO ₄ ²⁻ : 5.24×10^8	CO ₂ (g): 5.24×10^8 H ₂ S(g): 2.62×10^8	C: 0 SO ₄ ²⁻ : unknown
$C_6H_{10}O_5 + H_2O(l) \rightarrow 3CH_4(g) + 3CO_2(g)$			
C: 5.24×10^8	C: 5.24×10^8	CO ₂ (g): 2.62×10^8 CH ₄ (g): 2.62×10^8	C: 0
$Fe(s) + H_2O(l) + CO_2(g) \rightleftharpoons FeCO_3(s) + H_2(g)$			
Fe: 9.2×10^8 CO ₂ (g): 8.39×10^8	Fe: 8.39×10^8 CO ₂ (g): 8.39×10^8	FeCO ₃ (s): 8.39×10^8 H ₂ (g): 8.39×10^8	Fe: 8.4×10^7 CO ₂ (g): 0
$FeCO_3(s) + H_2S(g) \rightleftharpoons FeS(s) + H_2O(l) + CO_2(g)$			
FeCO ₃ (s): 8.39×10^8 H ₂ S(g): 2.62×10^8	FeCO ₃ (s): 2.62×10^8 H ₂ S(g): 2.62×10^8	FeS(s): 2.62×10^8 CO ₂ (g): 2.62×10^8	FeCO ₃ (s): 5.8×10^8 H ₂ S(g): 0
$Fe(s) + H_2O(l) + CO_2(g) \rightleftharpoons FeCO_3(s) + H_2(g)$			
Fe: 8.4×10^7 CO ₂ (g): 2.62×10^8	Fe: 8.4×10^7 CO ₂ (g): 8.4×10^7	FeCO ₃ (s): 8.4×10^7 H ₂ (g): 8.4×10^7	Fe: 0 CO ₂ (g): 1.8×10^8

Case 2: The CPR Carbon Remaining After Denitrification Reacts With Sulfates and Then With Water to Form CH₄

Calculations similar to those conducted for Case 1 were performed, with the additional assumption that the CPR carbon remaining unreacted after denitrification (i.e. 1.05×10^9 mol of C) will react with the entire waste sulfate inventory (4.61×10^6 mol SO₄²⁻) but with none of the sulfate contained in the marker beds or the brines. The remaining CPR carbon will then react to produce CH₄. Denitrification produces 5.39×10^7 mol of CO₂(g) and 2.16×10^7 mol of N₂(g) leaving 1.05×10^9 mol of CPR carbon unreacted. Sulfate reduction will produce 9.22×10^6 mol of CO₂(g) and 4.61×10^6 mol H₂S(g), and methanogenesis will produce 5.19×10^8 mol each of CH₄(g) and CO₂(g). Thus, a total of 5.82×10^8 mol of CO₂(g) can then react with metallic Fe to form 5.8×10^8 mol each of FeCO₃(s) and H₂(g), leaving 3.4×10^8 mol of Fe(s) unreacted. The reaction between FeCO₃(s) and H₂S(s) produces 4.6×10^6 mol each of FeS(s) and CO₂(g). This newly generated CO₂(g) can then react with the remaining Fe(s) to form an additional 4.6×10^6 mol of FeCO₃(s), consuming all of the available CO₂(g) and leaving 3.4×10^8 mol of Fe(s) unreacted. These calculations are summarized in Table 6.

Table 6. Summary of Results for Fe-Gas Reactions with the Denitrification, Sulfate Reduction, and Methanogenesis Processes, Case 2.

Material available (mol)	Reactants (mol)	Products (mol)	Unreacted Materials (mol)
$C_6H_{10}O_5 + 4.8H^+ + 4.8NO_3^- \rightarrow 7.4H_2O(l) + 6CO_2(g) + 2.4N_2(g)$			
C: 1.10×10^9 NO ₃ ⁻ : 4.31×10^7	C: 5.39×10^7 NO ₃ ⁻ : 4.31×10^7	CO ₂ (g): 5.39×10^7 N ₂ (g): 2.16×10^7	C: 1.05×10^9 NO ₃ ⁻ : 0
$C_6H_{10}O_5 + 6H^+ + 3SO_4^{2-} \rightarrow 5H_2O(l) + 6CO_2(g) + 3H_2S(g)$			
C: 1.05×10^9 SO ₄ ²⁻ : 4.61×10^6	C: 9.22×10^6 SO ₄ ²⁻ : 4.61×10^6	CO ₂ (g): 9.22×10^6 H ₂ S(g): 4.61×10^6	C: 1.04×10^9 SO ₄ ²⁻ : 0
$C_6H_{10}O_5 + H_2O(l) \rightarrow 3CH_4(g) + 3CO_2(g)$			
C: 1.04×10^9	C: 1.04×10^9	CO ₂ (g): 5.19×10^8 CH ₄ (g): 5.19×10^8	C: 0
$Fe(s) + H_2O(l) + CO_2(g) = FeCO_3(s) + H_2(g)$			
Fe: 9.2×10^8 CO ₂ (g): 5.82×10^8	Fe: 5.8×10^8 CO ₂ (g): 5.8×10^8	FeCO ₃ (s): 5.8×10^8 H ₂ (g): 5.8×10^8	Fe: 3.4×10^8 CO ₂ (g): 0
$FeCO_3(s) + H_2S(g) = FeS(s) + H_2O(l) + CO_2(g)$			
FeCO ₃ (s): 5.8×10^8 H ₂ S(g): 4.61×10^6	FeCO ₃ (s): 4.6×10^6 H ₂ S(g): 4.6×10^6	FeS(s): 4.6×10^6 CO ₂ (g): 4.6×10^6	FeCO ₃ (s): 5.8×10^8 H ₂ S(g): 0
$Fe(s) + H_2O(l) + CO_2(g) = FeCO_3(s) + H_2(g)$			
Fe: 3.4×10^8 CO ₂ (g): 4.6×10^6	Fe: 4.6×10^6 CO ₂ (g): 4.6×10^6	FeCO ₃ (s): 4.6×10^6 H ₂ (g): 4.6×10^6	Fe: 3.4×10^8 CO ₂ (g): 0

7.5.2 Pb Impact on Microbial Gases

The densities of Pb within the WIPP originating from the containers for CH and RH wastes have been estimated by Crawford to be 1.3×10^{-2} and 4.2×10^2 kg/m³, respectively (Crawford, 2005a). Therefore, considering the CH and RH volumes of 1.69×10^5 and 7080 m³, respectively (U.S. Congress, 1992), the total masses of Pb from the CH and RH waste containers are 2.2×10^3 and 3.0×10^6 kg, respectively. Crawford also estimated the total quantity of Pb and cadmium metal present within the "lead/cadmium" waste stream for both CH and RH wastes at closure time (Crawford, 2005b). As no differentiation was made between Pb and cadmium for the data discussed above, for this study we will assume that the total quantity is exclusively Pb. Although more Pb may be present in the WIPP from sources other than the "lead/cadmium" waste stream, this contribution to the total quantity has not been quantified, and thus will be neglected here. As a result, by considering only material contributed by the "lead/cadmium" waste stream, the estimated quantity from this calculation represents the lower limit of Pb present within the WIPP at closure. From Crawford, the estimated volumes of Pb within the CH and RH wastes are 2.6×10^2 and 19 m³, respectively, yielding associated densities of 1.5×10^2 kg/m³ and 74 kg/m³ (Crawford, 2005b). Therefore, the Pb masses contained in the CH and RH wastes are 3.9×10^4 and 1.4×10^3 kg, respectively. Combining the above information, the lower limit of the total quantity of Pb within the WIPP at closure is estimated to be 3.0×10^6 kg (1.5×10^7 mol), which translates to 17 mol of Pb per equivalent drum.

The maximum quantity, or upper limit, of Pb present within the WIPP can be estimated by using the density of the material denoted as "other metal/alloys" in the CH and RH wastes. This category contains all of the metals present in the wastes with the exception of Fe and aluminum, and has been estimated to be 32 and 57 kg/m³ for CH and RH waste, respectively (Crawford, 2005a). Applying this to the volumes of CH and RH waste, the maximum quantity which may present within the WIPP at closure time is 8.6×10^6 kg (4.2×10^7 mol), or 49 mol of Pb per equivalent drum.

7.5.2.1 DENITRIFICATION, SULFATE REDUCTION, NO METHANOGENESIS

Calculations similar to those developed in section 7.5.1.1 for Fe were performed for Pb. The denitrification process generates 5.39×10^7 and 2.16×10^7 mol of CO₂(g) and N₂(g), respectively and 1.05×10^9 mol of CPR carbon is left unreacted. In absence of methanogenesis, all the unreacted C reacts with sulfate and form 1.05×10^9 mol of CO₂(g) and 5.24×10^8 mol of H₂S(g). Then 1.10×10^9 mol of CO₂(g) is available to react with Pb(s) to generate 1.5×10^7 mol of each PbCO₃(s) and H₂(g), leaving 1.1×10^9 mol of unreacted CO₂(g). The reaction between PbCO₃(s) and H₂S(g) generates 1.5×10^7 mol of each PbS(s) and CO₂(g). Finally, a total of 1.1×10^9 mol of CO₂(g) is available to react with MgO. These calculations are summarized in Table 7.

Table 7. Summary of the Result of Pb-Gas Reactions with Denitrification and Sulfate Reduction Processes, and Without Methanogenesis.

Material available (mol)	Reactants (mol)	Products (mol)	Unreacted Materials (mol)
$C_6H_{10}O_5 + 4.8H^+ + 4.8NO_3^- \rightarrow 7.4H_2O(l) + 6CO_2(g) + 2.4N_2(g)$			
C: 1.10×10^9 NO ₃ ⁻ : 4.31×10^7	C: 5.39×10^7 NO ₃ ⁻ : 4.31×10^7	CO ₂ (g): 5.39×10^7 N ₂ (g): 2.16×10^7	C: 1.05×10^9 NO ₃ ⁻ : 0
$C_6H_{10}O_5 + 6H^+ + 3SO_4^{2-} \rightarrow 5H_2O(l) + 6CO_2(g) + 3H_2S(g)$			
C: 1.05×10^9 SO ₄ ²⁻ : unknown	C: 1.05×10^9 SO ₄ ²⁻ : 1.05×10^9	CO ₂ (g): 1.05×10^9 H ₂ S(g): 5.24×10^8	C: 0 SO ₄ ²⁻ : unknown
$Pb(s) + H_2O(l) + CO_2(g) = PbCO_3(s) + H_2(g)$			
Pb: 1.5×10^7 CO ₂ (g): 1.10×10^9	Pb: 1.5×10^7 CO ₂ (g): 1.5×10^7	PbCO ₃ (s): 1.5×10^7 H ₂ (g): 1.5×10^7	Pb: 0 CO ₂ (g): 1.1×10^9
$PbCO_3(s) + H_2S(g) = PbS(s) + H_2O(l) + CO_2(g)$			
PbCO ₃ (s): 1.5×10^7 H ₂ S(g): 5.24×10^8	PbCO ₃ (s): 1.5×10^7 H ₂ S(g): 1.5×10^7	PbS(s): 1.5×10^7 CO ₂ (g): 1.5×10^7	PbCO ₃ (s): 0 H ₂ S(g): 5.1×10^8

7.5.2.2 DENITRIFICATION, SULFATE REDUCTION, AND METHANOGENESIS

As in the calculations performed for Fe presented in Section 7.5.1.2, two scenarios were considered. In the first case, we consider that an unknown amount of sulfate reacts with the CPR carbon and in the second, we consider solely the sulfate issued from the waste.

Case 1: 50% of the C Remaining After Denitrification Reacts With Sulfate And 50% Reacts With Water to From CH₄

Calculations similar to those developed in section 7.5.1.2 for Fe were performed for Pb. In this section, it is assumed that half of the remaining moles of CPR C left unreacted following denitrification (i.e. 5.24×10^8 mol) will react through sulfate reduction process and the other half

through methanogenesis. Denitrification produces 5.39×10^7 mol of $\text{CO}_2(\text{g})$ and 2.16×10^7 mol of $\text{N}_2(\text{g})$, leaving 1.05×10^9 mol of CPR carbon unreacted. Sulfate reduction will produce 5.24×10^8 mol of $\text{CO}_2(\text{g})$ and 2.62×10^8 mol $\text{H}_2\text{S}(\text{g})$ and methanogenesis will produce 2.62×10^8 mol of each $\text{CH}_4(\text{g})$ and $\text{CO}_2(\text{g})$. The resulting $\text{CO}_2(\text{g})$ can then react with metallic Pb to form 1.5×10^7 mol each of $\text{PbCO}_3(\text{s})$ and $\text{H}_2(\text{g})$, leaving 8.2×10^8 mol of $\text{CO}_2(\text{g})$ unreacted. The reaction between $\text{PbCO}_3(\text{s})$ and $\text{H}_2\text{S}(\text{s})$ produces 1.5×10^7 mol each of $\text{PbS}(\text{s})$ and $\text{CO}_2(\text{g})$. At this point, there is no additional metallic Pb to react with this newly generated $\text{CO}_2(\text{g})$ and the 8.2×10^8 mol of $\text{CO}_2(\text{g})$ generated can react with the engineered barrier as described previously. These calculations are summarized in Table 8.

Table 8. Result Summaries for Pb-Gas Reactions With Denitrification, Sulfate Reduction, and Methanogenesis Processes, Case 1.

Material available (mol)	Reactants (mol)	Products (mol)	Unreacted Materials (mol)
$C_6H_{10}O_5 + 4.8H^+ + 4.8NO_3^- \rightarrow 7.4H_2O(l) + 6CO_2(g) + 2.4N_2(g)$			
C: 1.10×10^9 NO ₃ ⁻ : 4.31×10^7	C: 5.39×10^7 NO ₃ ⁻ : 4.31×10^7	CO ₂ (g): 5.39×10^7 N ₂ (g): 2.16×10^7	C: 1.05×10^9 NO ₃ ⁻ : 0
$C_6H_{10}O_5 + 6H^+ + 3SO_4^{2-} \rightarrow 5H_2O(l) + 6CO_2(g) + 3H_2S(g)$			
C: 5.24×10^8 SO ₄ ²⁻ : unknown	C: 5.24×10^8 SO ₄ ²⁻ : 5.24×10^8	CO ₂ (g): 5.24×10^8 H ₂ S(g): 2.62×10^8	C: 0 SO ₄ ²⁻ : unknown
$C_6H_{10}O_5 + H_2O(l) \rightarrow 3CH_4(g) + 3CO_2(g)$			
C: 5.24×10^8	C: 5.24×10^8	CO ₂ (g): 2.62×10^8 CH ₄ (g): 2.62×10^8	C: 0
$Pb(s) + H_2O(l) + CO_2(g) = PbCO_3(s) + H_2(g)$			
Pb: 1.5×10^7 CO ₂ (g): 8.39×10^8	Pb: 1.5×10^7 CO ₂ (g): 1.5×10^7	PbCO ₃ (s): 1.5×10^7 H ₂ (g): 1.5×10^7	Pb: 0 CO ₂ (g): 8.2×10^8
$PbCO_3(s) + H_2S(g) = PbS(s) + H_2O(l) + CO_2(g)$			
PbCO ₃ (s): 1.5×10^7 H ₂ S(g): 2.62×10^8	PbCO ₃ (s): 1.5×10^7 H ₂ S(g): 1.5×10^7	PbS(s): 1.5×10^7 CO ₂ (g): 1.5×10^7	PbCO ₃ (s): 0 H ₂ S(g): 2.5×10^8

Case 2: The C Remaining After Denitrification Reacts With The Waste Sulfates And Then With Water to Form CH₄

Calculations similar to those developed in section 7.5.1.2 , Case 2 for Fe were performed for Pb: it is assumed that the remaining moles of CPR carbon left unreacted following

denitrification (i.e. 1.05×10^9 mol of C) will react with the entire waste sulfate inventory, but with none of the sulfate of the marker beds or brines; the inventory contains 4.61×10^6 mol SO_4^{2-} . The remaining CPR carbon will then react to form CH_4 . Denitrification produces 5.39×10^7 mol of $\text{CO}_2(\text{g})$ and 2.16×10^7 mol of $\text{N}_2(\text{g})$ and leaves 1.05×10^9 mol of CPR carbon unreacted. Sulfate reduction will produce 9.22×10^6 mol of $\text{CO}_2(\text{g})$ and 4.61×10^6 mol $\text{H}_2\text{S}(\text{g})$ and methanogenesis will produce 5.19×10^8 mol of each $\text{CH}_4(\text{g})$ and $\text{CO}_2(\text{g})$. A total of 5.82×10^8 mol of $\text{CO}_2(\text{g})$ can then react with metallic Pb to form 1.5×10^7 mol of each $\text{PbCO}_3(\text{s})$ and $\text{H}_2(\text{g})$, leaving no unreacted Pb(s). The reaction between $\text{PbCO}_3(\text{s})$ and $\text{H}_2\text{S}(\text{s})$ produces 4.6×10^6 mol each of $\text{PbS}(\text{s})$ and $\text{CO}_2(\text{g})$. At this point, unlike Fe, there is no more metallic Pb to react with this newly generated $\text{CO}_2(\text{g})$ and the 5.7×10^8 mol of $\text{CO}_2(\text{g})$ generated can react with the engineered barrier as described previously. These calculations are summarized in Table 9.

Table 9. Result Summaries for Pb-Gas Reactions with Denitrification, Sulfate Reduction, and Methanogenesis Processes, Case 2.

Material available (mol)	Reactants (mol)	Products (mol)	Unreacted Materials (mol)
$C_6H_{10}O_5 + 4.8H^+ + 4.8NO_3^- \rightarrow 7.4H_2O(l) + 6CO_2(g) + 2.4N_2(g)$			
C: 1.10×10^9 NO ₃ ⁻ : 4.31×10^7	C: 5.39×10^7 NO ₃ ⁻ : 4.31×10^7	CO ₂ (g): 5.39×10^7 N ₂ (g): 2.16×10^7	C: 1.05×10^9 NO ₃ ⁻ : 0
$C_6H_{10}O_5 + 6H^+ + 3SO_4^{2-} \rightarrow 5H_2O(l) + 6CO_2(g) + 3H_2S(g)$			
C: 1.05×10^9 SO ₄ ²⁻ : 4.61×10^6	C: 9.22×10^6 SO ₄ ²⁻ : 4.61×10^6	CO ₂ (g): 9.22×10^6 H ₂ S(g): 4.61×10^6	C: 1.04×10^9 SO ₄ ²⁻ : 0
$C_6H_{10}O_5 + H_2O(l) \rightarrow 3CH_4(g) + 3CO_2(g)$			
C: 1.04×10^9	C: 1.04×10^9	CO ₂ (g): 5.19×10^8 CH ₄ (g): 5.19×10^8	C: 0
$Pb(s) + H_2O(l) + CO_2(g) \rightleftharpoons PbCO_3(s) + H_2(g)$			
Pb: 1.5×10^7 CO ₂ (g): 5.82×10^8	Pb: 1.5×10^7 CO ₂ (g): 1.5×10^7	PbCO ₃ (s): 1.5×10^7 H ₂ (g): 1.5×10^7	Pb: 0 CO ₂ (g): 5.7×10^8
$PbCO_3(s) + H_2S(g) \rightleftharpoons PbS(s) + H_2O(l) + CO_2(g)$			
PbCO ₃ (s): 1.5×10^7 H ₂ S(g): 4.61×10^6	PbCO ₃ (s): 4.6×10^6 H ₂ S(g): 4.6×10^6	PbS(s): 4.6×10^6 CO ₂ (g): 4.6×10^6	PbCO ₃ (s): 9.9×10^6 H ₂ S(g): 0

7.6 Summary of the Results of Interactions of Fe and Pb with Microbially Generated Gases

Table 10 summarizes the results presented in sections 7.5.1 and 7.5.2. The table presents the quantity of carbon involved in each of the microbial gas generation process: denitrification, sulfate reduction and methanogenesis, and for each of the sulfate scenarios, where the sulfate

involved in the sulfate reduction is issued either from the waste or from the waste and the WIPP structure (marker beds and brines). If we assume that sulfate from both the waste and the WIPP structure are available for reaction, and that the only viable carbon consumption pathways are denitrification (Eqn. 7) and sulfate reduction (Eqn. 8), then 95% of the CPR carbon will be consumed via sulfate reduction. Under those same conditions, if we add methanogenesis (Eqn. 9) as an additional consumption pathway for the CPR carbon, the quantity consumed by sulfate reduction falls to 48%. Finally, if we then neglect sulfate originating from the WIPP structure, and consider only the sulfate within the waste, then just 1% of the CPR carbon will be consumed via sulfate reduction.

Table 10 also shows the quantity of gases produced from the reactions taking place between metallic Fe and Pb and the gases generated by microbial activities. The amount of $\text{CO}_2(\text{g})$ generated from the reaction between metallic Fe or Pb with the microbially generated gas decreases as the amount of carbon consumed through methanogenesis increases. This is due to the fact that, for a fixed amount of carbon, sulfate reduction generates twice as much $\text{CO}_2(\text{g})$ as methanogenesis. In the absence of methanogenesis, the reaction of metallic Fe and Pb with the microbially generated gases produces 7.0×10^8 and 1.1×10^9 mol of $\text{CO}_2(\text{g})$, respectively. With 48 % of carbon consumed through methanogenesis, these numbers decrease to 1.8×10^8 and 8.4×10^8 mol of $\text{CO}_2(\text{g})$, respectively. The only case where $\text{CO}_2(\text{g})$ produced by microbial activity and metal corrosion is completely consumed is for Fe corrosion after 94 % of the CPR carbon has been consumed through methanogenesis. Of course, $\text{CH}_4(\text{g})$ generation increases as the amount of carbon involved in methanogenesis increases. The amount of $\text{N}_2(\text{g})$ does not vary with methanogenesis as it is only produced through the denitrification process. Finally, the only case in which $\text{H}_2(\text{g})$ varies is when the $\text{CO}_2(\text{g})$ is completely consumed before metallic Fe is consumed. In this case, 5.9×10^8 mol of $\text{H}_2(\text{g})$ is then produced. Otherwise, 9.2×10^8 and 1.5×10^7 mol of $\text{H}_2(\text{g})$ are produced from the corrosion of Fe and Pb, respectively.

Table 10. Percentage of Carbon Involved in the Microbial Gas Generation Reactions and Moles of Gases Generated from the Reactions between Metallic Fe and Pb and the Microbially Generated Gas.

Origin of sulfate	No Methanogenesis		With Methanogenesis			
	Waste and WIPP		Waste and WIPP		Waste	
	Fe	Pb	Fe	Pb	Fe	Pb
CPR C consumed by:						
• Denitrification	5 %		4.5 % ¹		5 %	
• Sulfate Reduction	95 %		47.6 % ¹		1 %	
• Methanogenesis	0 %		47.6 % ¹		94 %	
Gases Produced and unreacted metals:						
CO ₂ (g) (mol)	7.0 × 10 ⁸	1.1 × 10 ⁹	1.8 × 10 ⁸	8.4 × 10 ⁸	0	5.7 × 10 ⁸
CH ₄ (g) (mol)	0	0	2.6 × 10 ⁸	2.6 × 10 ⁸	5.2 × 10 ⁸	5.2 × 10 ⁸
N ₂ (g) (mol)	2.2 × 10 ⁷					
H ₂ (g) (mol)	9.2 × 10 ⁸	1.5 × 10 ⁷	9.2 × 10 ⁸	1.5 × 10 ⁷	5.9 × 10 ⁸	1.5 × 10 ⁷
H ₂ S(g) (mol)	0	5.1 × 10 ⁸	0	2.5 × 10 ⁸	0	0
Unreacted metal (mol)	0	0	0	0	3.4 × 10 ⁸	0

7.7 Additional Aspects on the Influence of Fe and Pb on the System

In addition to forming a number of new solid phases, Fe and Pb will also influence the solution compositions as they slowly dissolve in the aqueous phase. Two brines will be considered in this study. The first, simulating fluids present within reservoirs in the Castile Formation, is the ERDA-6 brine. The other brine is the GWB which simulates intergranular brines from the Salado formation at or near the stratigraphic horizon of the repository. These brines, which will be discussed in more detail in Section 9.2.1, contain inorganic ligands, such as SO₄²⁻, Cl⁻, and HCO₃⁻ that will complex to the soluble species of Fe and Pb and therefore change

¹ Percentage rounding explains that the sum is not 100%.

the brine composition. Moreover, the WIPP waste will contain significant amount of acetate, oxalate, citrate, and ethylenediaminetetraacetic acid (EDTA), at closure time, as discussed later in this document in the section 9.1.3 . For example, acetate, oxalate, citrate, and EDTA will form complexes with Fe^{2+} , with the following stability constant of the first complexes: $10^{1.4}$ (at 0 M ionic strength), $10^{3.05}$ (at 1.0 M ionic strength), $10^{4.4}$ (at 0.1 M ionic strength), $10^{14.30}$ (at 0.1 M ionic strength), respectively (Martell et al., 1998). Pb^{2+} will also form complexes with those ligands; the stability constant of the first complexes with oxalate, citrate, and EDTA are $10^{4.20}$ (at 1.0 ionic strength), $10^{4.44}$ (at 1.0 ionic strength), and $10^{18.0}$ (at 0.1 ionic strength), respectively (Martell et al., 1998). As a comparison, the first stability constants of the complexes formed between americium (Am) and acetate, oxalate, citrate, and EDTA are $10^{1.51}$, $10^{4.17}$, $10^{5.2}$, and $10^{13.96}$, respectively, at 1.0 M ionic strength (Choppin et al., 2001).

8 REVIEW OF DATA FOUND ON CORROSION IN THE WIPP

There have been a number of studies which have, at least peripherally, evaluated the corrosion behavior of Fe and Pb alloys under WIPP relevant conditions. One such study was performed by Telander and Westerman beginning in 1989 and ending in 1996 (Telander and Westerman, 1993; 1997). Their study focused on determining the quantity of gas generation (specifically H₂ from water reduction) which would result from the corrosion process. Carbon steel (both hot and cold rolled material), along with a series of other nonferrous alloys were evaluated in Brine A and ERDA-6 with overpressures of N₂, CO₂, H₂, and H₂S (both singularly and in combinations). In their study, it was found that there was no statistically significant difference in behavior between the two different steels under any of the conditions evaluated – as such, the results for all of the Fe alloys were combined and averaged. Considerable H₂ production was observed in most of the test cases – however, though the corrosion rate of carbon steel did seem to decrease for moderate H₂ pressures (36 to 70 atm), they stated that the overall impact of H₂ overpressure on the corrosion rate of low carbon steels was insignificant in the long run, even at pressures as high as the lithostatic pressure.

Under a N₂ overpressure, which creates an O₂ depleted environment, samples immersed in Brine A exhibited a corrosion rate of 0.71 μm/yr. The resulting corrosion product was found to be an iron-magnesium hydroxide. Samples exposed to the vapor phase over the brine showed no discernable corrosion. In the ERDA-6 brine, the corrosion rate was found to be highly dependant on the pH of the brine, ranging from 7.9 mm/yr at pH 5 to 2 μm/yr at pH 9.

When a CO₂ overpressure was applied, samples were observed to passivate in Brine A due to the formation of protective layer of FeCO₃ or Fe₂Mn(CO₃)₂. The passivation process was found to require a minimum concentration of CO₂ in the gas phase somewhere between 0.16 and 0.32 mol CO₂/m² of steel. The steel could also be depassivated by the addition of H₂S, after which repassivation did not occur, and corrosion continued as if the samples were exposed to anoxic brine. Samples were also exposed to the vapor phase over the brine, where again no significant attack was observed.

With an overpressure of H₂S, the steel samples were again observed to passivate, with the formation of a protective iron sulfide layer (FeS). Addition of small concentrations of CO₂ to the gas mixture did not disrupt the passive layer.

Another test program which was conducted under WIPP relevant conditions was the Materials Interface Interactions Test (MIIT) performed by Molecke, et. al. (1993) The goal of that work was to evaluate the behavior of a wide range of materials, including several carbon steels (American Society for Testing and Materials (ASTM) A216 grade WCA and a Belgian carbon steel) and a Pb alloy, to WIPP relevant conditions. In this test, samples were emplaced within boreholes in room J and nominally exposed to Brine A which had equilibrated with the surrounding salt. The gas composition within the boreholes (which were mostly filled with brine) was not controlled, and did not contain the mixture of microbially generated gasses which are being explored in this proposal. Samples were monitored periodically for 5 years, and a qualitative assessment of the corrosion performance was given. In the case of the carbon steels, all samples demonstrated significant general and localized attack, with voluminous corrosion

product being produced (the composition was not determined). The Pb samples also underwent significant general and localized attack, though there was more sample to sample variability. As with the steel, the composition of the corrosion products was not analyzed.

One final test program which focused in understanding the mechanism of Fe corrosion in WIPP brines was performed by Wang, et. al (Wang, 2001). In this study, A36 cold rolled steel sheet was evaluated in G Seep and ERDA-6 brines which had been equilibrated for 7 days with $Mg(OH)_2$. While they were not able to elucidate the finer points of the corrosion process due to experimental limitations, they were able to characterize the corrosion product which resulted on the steel coupons. In this case, a green rust was produced (a layered (Fe(II), Fe(III)) hydroxide with water and anions such as chloride and sulfate occupying the interlayer spaces.

Xia et al. (2001) studied the effect of Fe on the plutonium, neptunium, and uranium solubilities and oxidation states in NaCl solutions and in ERDA-6. But they did not discuss the Fe corrosion occurring during the experiments.

9 EXPERIMENTAL PROCESS DESCRIPTION

As discussed above, the goal of this proposed research is to determine the likely corrosion products which will result due to oxidation of the Fe and Pb contained within the WIPP. A mixed flowing gas exposure system will be constructed which allows for the simulation of the predicted in-room atmosphere within the WIPP. Exposure testing will then be performed on a number of relevant materials, after which the resulting aged surfaces will be quantitatively assessed via an array of analytical techniques.

9.1 Materials

9.1.1 Alloys

Several ferrous and non-ferrous materials were selected for evaluation in this study. Two Fe-base alloys, representative of the container materials used for CH waste along with a Pb alloy representative of potential shielding material for RH waste were selected. The text below describes the reasoning used to select the relevant alloys, along with their compositions.

9.1.1.1 Fe-BASE ALLOYS

CH waste within the WIPP is in general disposed in one of four different forms – drums (55, 85, and 100 gallons in size), standard waste boxes (Golden, 2004a), ten drum overpacks (Golden, 2004b), or standard large boxes (Golden, 2005). The materials of construction, as well as the anticipated quantity (Burns, 2005), of each storage container is presented in Table 11. The materials of construction are specified in a series of ASTM specifications, as shown in Table 12. These specifications each encompass a range of different carbon and high-strength, low-alloy (HSLA) steels. From Table 11, it is clear that the majority of the steel present in the WIPP (from waste containers) will be of a composition as defined either by ASTM A36, ASTM A1008, or ASTM A1011, with the largest quantity defined by ASTM A1008 (waste drums). The steels specified in A1008 and A1011 are similar (see Table 12) with the exception of the method of production, with the former being cold-rolled, and the latter hot-rolled. While this will yield different mechanical properties in the final product, it has been found previously by Telander and Westerman (Telander and Westerman, 1993; 1997) that the two will behave similarly from a corrosion point of view in brines of a composition relevant to the WIPP. As such, only one of them will be selected for evaluation in this study (ASTM A1008), along with a material which conforms to ASTM A36.

Table 11. Materials of Construction for the Various Waste Containers.

ASTM Specification →	A29	A36	A108	A266	A500	A510	A513	A516	A537	A576	A865	A1008	A1011	F835	SAE grade 5	ASME/ANSI B1.20.1	# in WIPP
Standard Waste Box																	17031
Body panels, Lid panel													X				
Body tubular frame; body bumper							X										
Body clips; lid frame bar		X															
Rivets						X				X							
Lid lift nut	X	X				X				X							

Table 11. Materials of Construction for the Various Waste Containers (cont.).

ASTM Specification →	A29	A36	A108	A266	A500	A510	A513	A516	A537	A576	A865	A1008	A1011	F835	SAE grade 5	ASME/ANSI B1.20.1	# in WIPP
Ten Drum Overpack																	7138
Body panels; body lift clip; lid panel; lid band		X															
Body flange				X				X	X								
Body bumper							X										
Spacer							X										
Lift nut	X	X				X				X							
Socket head cap screws														X			
Waste Drums																	
55, 85, and 100 Gallon Drums												X					396719

Table 11. Materials of Construction for the Various Waste Containers (cont.).

ASTM Specification →	A29	A36	A108	A266	A500	A510	A513	A516	A537	A576	A865	A1008	A1011	F835	SAE grade 5	ASME/ANSI B1.20.1	# in WIPP
Standard Large Box 2																	1818
Body shell, wall, flange, gusset, vertical spacer, corner brace; lift clip; lid panel		X															
Body labyrinth side and end; bumper cap; lid labyrinth side and end; lid skid cap													X				
Gasket compression lug	X					X											
Pipe coupling, half											X						
Hex flange bolt and nut															X		
Coupling pipe plug																X	

Table 12. Material Compositions Defined by ASTM Specifications (all compositions in wt %).

Specification		C	Mn	P	S	Si	Cu	Ni	Cr	Mo	V	Cd	Ti
A29	Grade 1018	0.15-0.20	0.60-0.90	0.04 max	0.05 max	0.1 max							
A36		0.26 max		0.04 max	0.05 max	0.4 max	0.2 min (if specified)						
A108	calls out A29 or A510												
A266	grade 3 normalized	0.35 max	0.8-1.05	0.025 max	0.025 max	0.15-0.35							
A500	unspecified Grade	0.27-0.30 max	1.40 max	0.045 max	0.045 max		0.18 min (if specified)						
A510	Grade 1008	0.10 max	0.25-0.40	0.04 max	0.05 max								
	Grade 1010	0.08-0.13	0.30-0.60	0.04 max	0.05 max								
	Grade 1018	0.15-0.20	0.60-0.90	0.04 max	0.05 max								
	Grade 1110	0.08-0.13	0.30-0.60	0.04 max	0.08-0.13	0.10 max							

Table 12. Material Compositions Defined by ASTM Specifications (cont.).

Specification		C	Mn	P	S	Si	Cu	Ni	Cr	Mo	V	Cd	Ti
A513	Grade 1008	0.1 max	0.5 max	0.035 max	0.035 max								
	Grade 1010	0.08-0.13	0.30-0.60	0.035 max	0.035 max								
	Grade 1012	0.1-0.15	0.30-0.60	0.035 max	0.035 max								
	Grade 1015	0.12-0.18	0.30-0.60	0.035 max	0.035 max								
	Grade 1016	0.12-0.18	0.60-0.90	0.035 max	0.035 max								
	Grade 1017	0.14-0.20	0.30-0.60	0.035 max	0.035 max								
	Grade 1018	0.14-0.20	0.60-0.90	0.035 max	0.035 max								
	Grade 1019	0.14-0.20	0.70-1.00	0.035 max	0.035 max								
	Grade 1020	0.17-0.23	0.30-0.60	0.035 max	0.035 max								
A516	grade 70 Normalized	0.27 max	0.85-1.20	0.035 max	0.035 max	0.15-0.45							
A537	Class 1	0.24 max	0.64-1.46	0.035 max	0.035 max	0.13-0.55	0.38 max	0.28 max	0.29 max	0.09 max			

Table 12. Material Compositions Defined by ASTM Specifications (cont.).

Specification		C	Mn	P	S	Si	Cu	Ni	Cr	Mo	V	Cd	Ti
A576	Grade 1008	0.10 max	0.30-0.50	0.04 max	0.05 max								
	Grade 1010	0.08-0.13	0.30-0.60	0.04 max	0.05 max								
	Grade 1018	0.15-0.20	0.60-0.90	0.04 max	0.05 max								
	Grade 1110	0.08-0.13	0.30-0.60	0.04 max	0.08-0.13	0.10 max							
A865				0.14 max	0.35 max								
A1011	Grade 30 (min)	0.25 max	1.35 max	0.035 max	0.040 max		0.2 max	0.2 max	0.15 max	0.06 max	0.008 max	0.008 max	0.025 max
A1008	unspec grade												
F835		0.30-0.48		0.035 max	0.040 max								

Table 13. ASTM Specifications.

ASTM Specification	Title
A29	Standard Specification for Steel Bars, Carbon and Alloy, Hot-Wrought, General Requirements for
A36	Standard Specification for Carbon Structural Steel
A108	Standard Specification for Steel Bar, Carbon and Alloy, Cold Finished
A266	Standard Specification for Carbon Steel Forgings for Pressure Vessel Components
A500	Standard Specification for Cold-Formed Welded and Seamless Carbon Steel Structural Tubing in Rounds and Shapes
A510	Standard Specification for General Requirements for Wire Rods and Coarse Round Wire, Carbon Steel
A513	Standard Specification for Electric-Resistance-Welded Carbon and Alloy Steel Mechanical Tubing
A516	Standard Specification for Pressure Vessel Plates, Carbon Steel, for Moderate- and Lower Temperature Service
A537	Standard Specification for Pressure Vessel Plates, Heat Treated, Carbon-Manganese-Silicon Steel
A576	Standard Specification for Steel Bars, Carbon, Hot-Wrought, Special Quality
A865	Standard Specification for Threaded Couplings, Steel, Black or Zinc Coated Welded or Seamless, for use in Steel Pipe Joints
A1011	Standard Specification for Steel Sheet and Strip, Hot Rolled, Carbon, Structural, High-Strength, Low-Alloy, and High-Strength Low Alloy with Improved Formability
A1008	Standard specification for steel, sheet, cold-rolled, carbon, structural, high-strength Low-Alloy, High-Strength Low-Alloy with Improved Formability, Solution Hardenable, and Bake Hardenable
F835	Standard specification for alloy steel socket button and flat countersunk head cap screws

9.1.1.2 Pb-BASE METALS

The estimated quantity of Pb present in the repository as a result of the waste and its containers is 3.0×10^6 kg (see Section 7.5.2). Only 1.4 % of this Pb mass is from the Pb present in the waste itself; the vast majority is due to the Pb contained in the lid of the packaging. The drawings for the RH containers (Hertelendy, 1984) do not specify the Pb alloy used.

The WIPP is planning to use Pb-lined containers for on-site storage of high radiation dose rate (i.e. RH) waste. There are six different container sizes which will be used, listed in Table 14. The nominal mass of Pb resulting from these containers is 4.4×10^6 kg, assuming that the Pb is at the external edge of the container. The Pb-lined containers are currently planned to be used exclusively for on-site storage. But in the event that they are disposed underground, the WIPP Pb inventory would increase. Several specifications are called out for the specific Pb alloy – namely military specification QQ-L-171e, which in turn calls ASTM B29. The specific grade of Pb required has not been defined. As such, referring to the mil spec, Grade C is specified for chemical use, and is what will be used here. This alloy is defined in ASTM B29 as chemical-copper lead (UNS L51121) and is nominally 99.9% Pb.

Table 14. Size and Number of the Pb-Lined Containers.

Container ID	Pb-lined thickness (nom. in.) ¹	External Height (in.) ¹	External Diameter (in.) ¹	Projected Number in WIPP ²
TS55-PB2	2	34 ¼	24	1200
TS55-PB3	3	34 ¼	24	1200
TS85-PB2	2	39 ¼	27	150
TS85-PB3	3	39 ¼	27	150
TS110-PB2	2	43	31	150
TS146-PB3	3	43	33	150

¹ Bull Run Metal (2004)

² Woolsey (2005)

9.1.2 Gas Composition

9.1.2.1 CARRIER GAS

As discussed previously, with time it has been postulated that bacteria may consume the CPR materials within the WIPP, resulting in the production of large quantities of various gasses (see Equations (7), (8) and (9)), namely CH_4 , CO_2 , and H_2S . In addition, it is anticipated, based upon the results of Telander and Westerman discussed above, that considerable H_2 will be produced via the corrosion process. Due to their flammable natures, the use of either H_2 or CH_4 in the experimentation described within this test plan presents serious environmental health and safety concerns. As such, it is desirable that an alternative carrier gas be identified. In order to make such a replacement, the impact which each of these gases would have on the materials of concern in this study must be considered.

The storage containers utilized within the WIPP are constructed primarily from a variety of carbon and HSLA steels. In the study performed by Telander and Westerman, these materials were exposed to environments containing various concentrations of the gas species described above, including H_2 . In terms of the impact which H_2 had on the corrosion rate of these materials, they concluded that while there appeared to be a minor influence as the partial pressure of H_2 increased, that the overall impact in the long term would be negligible. As such, use of H_2 as a major component of the carrier gas is not necessary.

For CH_4 , steels compositionally similar to those found within the WIPP are widely used in natural gas transmission and are specified for such applications by the Pipeline and Hazardous Materials Safety Administration's Office of Pipeline Safety (the federal safety authority for natural gas pipelines). The DOT specifies that the materials used in such gas transmission lines conform to ASTM A53. Looking at that specification, it can be seen that all of the materials utilized within the steel WIPP storage containers also conform to the rather broad compositional range defined within ASTM A53. While CH_4 has been found to inhibit corrosion to a degree in carbon steels in deoxygenated Salton Sea brines at 232°C within a glass lined autoclave (Cramer, 1980), there is no data in the literature indicating that such an effect extends to the temperatures of interest in this study. As such, it is reasonable to assume that for the temperature and pressure regimes of concern here, the steel is effectively inert in this environment. Thus any replacement chemistry must be similarly inert. One such gas which is easily handled and readily available is N_2 , which consequently will be used in this study as the carrier gas.

9.1.2.2 CO_2 CONCENTRATION

Several approaches were used to determine an appropriate range of $\text{CO}_2(\text{g})$ concentrations to be evaluated in this study. The thermodynamic calculations performed in Section 7 demonstrated that if all the carbon from the CPR materials projected to be emplaced within the WIPP was consumed by microbial activity, it would yield a total of 1.10×10^9 , 8.39×10^8 , and 5.82×10^8 mol of $\text{CO}_2(\text{g})$, in the absence of methanogenesis, with 48% of the CPR carbon consumed by methanogenesis, and with 94% of the CPR carbon consumed by methanogenesis, respectively. Assuming a headspace volume in the WIPP of $26,000 \text{ m}^3$ (Stein, 2005), and using the gas molar volume of 22.4 L (at the standard condition of temperature and

pressure, i.e. 0°C and 1 atm), these quantities of CO₂(g) result in internal pressures of 950, 720, and 500 atm., respectively. It should be noted that these values are projected generated quantities, and do not account for consumption by the engineered barrier or metals within the WIPP.

Francis et al. (1997) performed experiments to evaluate the quantity and rate of CO₂(g) generation by microbes under WIPP relevant conditions. Nemer et al. (2005) utilized Francis' data to calculate the rate of gas generation within the WIPP. The maximum CO₂(g) generation rates were found to be 0.459 and 2.015×10^{-2} μmol CO₂/g cellulose/day, for periods of time shorter than 500 days and for long term, respectively. The minimum rates are 0.0115 and 5.57×10^{-3} μmol CO₂/g cellulose/day, for short (less than 500 days) and long term conditions, respectively. Francis' experiments were performed using 5 g of cellulose with a head space of 50 mL. Using the gas molar volume of 22.4 L, we deduce that after 500 days, the minimum and the maximum pressures of CO₂(g) were 0.013 and 0.514 atm, respectively. These numbers would yield pressures of 46 and 165 atm for a 10,000 years period (if the "long term" rate extend to 10,000 years), if the CO₂(g) was not consumed. In the presence of MgO, a portion of the CO₂(g) generated by the microbes is consumed to form a magnesium hydroxyl-carbonate, as shown in Equation (10). The resulting pressure of CO₂(g) following interaction with MgO was calculated to be $10^{-5.5}$ atm (Brush, 2005). We suspect that the kinetics of CO₂(g) consumption by MgO would not be overwhelmingly faster than that of CO₂(g) with Fe or Pb. Therefore, we will work with pressure of CO₂(g) greater than $10^{-5.5}$ atm (i.e. 3.6 ppm) but below 165 atm (i.e. 10^8 ppm). For example, we can work with the concentrations from 350 to 1,000 ppm.

9.1.2.3 H₂S CONCENTRATION

We have determined in Section 7 of this document that the sulfidization of the entire inventory of Fe and Pb would yield a ratio of CO₂(g) to H₂S(g) fugacities of $10^{2.44}$ and $10^{12.32}$, respectively (Equations (45) and (57)). Therefore, if the equilibrium fugacity of CO₂(g) is $10^{-5.5}$ atm (as calculated by Brush (2005) for a system containing MgO), the fugacity of H₂S(g) is $10^{-7.9}$ atm (i.e. 10^{-2} ppm) and $10^{-17.8}$ atm (i.e. 10^{-12} ppm), for Fe and Pb, respectively. Using the same argument as preceding section, we suspect that the kinetics of the reaction between CO₂(g) and MgO would not be overwhelmingly faster than that of CO₂(g) with Fe or Pb; therefore, the pressure of CO₂(g) will probably be higher than $10^{-5.5}$ atm for an extended period of time and in turn the pressure of H₂S(g) will be higher than $10^{-7.9}$ or $10^{-17.18}$ atm. If we maintain CO₂(g) at 350 ppm, as explained in the previous section, the H₂S(g) fugacity should be maintained at least at 1.3 and 2×10^{-10} ppm, for the Fe and Pb systems, respectively. But if CO₂(g) is maintained at 1,000 ppm, the H₂S(g) fugacity should be maintained at least at 3.6 and 5×10^{-10} ppm, for the Fe and Pb systems, respectively. However, as with CH₄, H₂S(g) presents significant environmental health and safety concerns – as such, to mitigate these concerns the Permissible Exposure Limit (PEL) for H₂S(g) is 20ppm (ceiling); exposure to 100ppm is immediately dangerous to life or health.

9.1.3 Presence of Organic Ligands in the Brine

The WIPP waste will contain significant amounts of acetate, citrate, EDTA, and oxalate, at closure time. Brush and Xiong (2005b) calculated the concentration of these ligands for the

WIPP PA baseline calculations (PABC); the results are presented in Table 15. These ligands are important to consider for the WIPP PA, as they influence the solubility of the actinides in the WIPP. Furthermore, the literature indicates that all of these species can have a significant impact on the electrochemical behavior of both Fe and Pb.

Table 15. Concentrations of Organic Ligands for a Homogeneous 10-Panel Repository.

Organic Ligand	Organic Ligand concentrations in PABC (M)
Acetate	1.06×10^{-2}
Citrate	8.06×10^{-4}
EDTA	8.14×10^{-6}
Oxalate	4.55×10^{-2}

In the case of steel, acetate has been found to enhance the dissolution rate in oilfield brines by stimulating cathodic activity at the Fe surface (Pletcher, 2005). Acetic acid has been found to similarly enhance the corrosion of Pb alloys. (Sankaeapapavinasam, 1989a) Conversely, both oxalic acid (Saltykov, 2004) and EDTA (Shukla, 2004) have been found to effectively inhibit the corrosion of carbon steels. Oxalic acid has also been found to inhibit corrosion on Pb alloys (Sankaeapapavinasam, 1989b). Finally, citric acid is widely used in the removal of corrosion product from Fe surfaces, where it readily complexes with Fe (Kubal, 1995).

While none of these studies have evaluated the impact which low concentrations will have in WIPP relevant brines, they do strongly suggest that the organic ligands may have an impact on the corrosion process. As such, they will be incorporated into the brines used in this study.

9.2 Tasks List

9.2.1 Task 1: Brine Preparation

The experiments will be performed using two WIPP-representative brines or some derivative of these brines. The two brines in questions are the ERDA-6, which represents fluids from reservoirs in the Castile Formation and the GWB, which represents intergranular brines from the Salado Formation at or near the stratigraphic horizon of the repository. The compositions of these brines are presented in Table 16. The preparation of these brines has been discussed elsewhere (Robinson, 1996; Snider, 2003).

Table 16. Compositions of GWB and ERDA-6 Prior to Equilibration with MgO.

Element or Property	GWB ¹	ERDA-6 ²
B(OH) _x ^{3-x}	158 mM	63 mM
Na ⁺	3.53 M	4.87 M
Mg ²⁺	1.02 M	19 mM
K ⁺	467 mM	97 mM
Ca ²⁺	14 mM	12 mM
SO ₄ ²⁻	177 mM	170 mM
Cl ⁻	5.86 M	4.8 M
Br ⁻	26.6 mM	11 mM
Total inorganic C (as HCO ₃ ⁻)	-	16 mM
pH	-	6.17
Sp. gr.	1.2	1.216

With time, a portion of the engineered barrier (MgO) will dissolve in the brine present within the WIPP, altering its composition. Brush (2005) published the compositions of both GWB and ERDA-6 brines following equilibration with MgO and in the presence of the anticipated concentration of organic ligands discussed in Section 9.1.3. These brine compositions were calculated for the PABC, using the geochemical speciation and solubility code Fracture-Matrix Transport (FMT) (Babb and Novak, 1997). The calculations were conducted with the assumption of instantaneous, reversible equilibria among GWB or ERDA-6, major Salado minerals such as halite (NaCl) and anhydrite (CaSO₄), and the MgO hydration and carbonation products Mg(OH)₂ and Mg₅(CO₃)₄(OH)₂·4H₂O buffering chemical conditions, such as f_{CO₂}, pH, and brine composition. These brine compositions are presented in Table 17.

¹ Snider, 2003

² Popielak et al., 1983

Table 17. Compositions of GWB and ERDA-6 after Equilibration with MgO, in the Presence of Organic Ligands (Brush, 2005).

Element or Property	GWB ¹	ERDA-6 ²
B(OH) _x ^{3-x}	70.0 mM	23.4 mM
Na ⁺	4.35 M	5.243 M
Mg ²⁺	0.503 M	138 mM
K ⁺	0.514 M	96.1 mM
Ca ²⁺	7.40 mM	9.08 mM
SO ₄ ²⁻	228 mM	179 mM
Cl ⁻	5.65 M	5.24 M
Br ⁻	27.8 mM	10.9 mM
Total inorganic C (as HCO ₃)	0.0422 mM	0.0790 mM
pH	8.69	8.94
Sp. gr.	1.23	1.22
Uncomplexed ³ Acetate	5.70 mM	6.97 mM
Uncomplexed Citrate	0.0173 mM	0.0189 mM
Uncomplexed EDTA	8.37 × 10 ⁻¹¹ M	1.74 × 10 ⁻¹¹ M
Uncomplexed Oxalate	0.0121 mM	0.00638 mM

However, these brine chemistries were calculated with a CO₂(g) partial pressure of 10^{-5.5} atm, which might not be appropriate for our experiments, as discussed above. We have chosen to use a higher P_{CO₂(g)} than 10^{-5.5} atm, as presented in Section 9.1.2. We will attempt to

¹ FMT run output 7

² FMT run output 11

³ Sum of the ligand concentration, as deprotonated or protonated, but not complexed to a metal.

calculate the brine compositions resulting from the equilibration of ERDA-6 and GWB with MgO, under a $P_{CO_2(g)}$ relevant to our experiments (e.g. 350 ppm), using the geochemical code FMT. Additionally, we will attempt to determine the brine composition resulting from the equilibrium of ERDA-6 and GWB with MgO, at pH higher and lower than pH 9. If successful, we will run experiments with the resulting brines. Brines may interact with steel and Pb alloys in the repository, prior to equilibration with MgO; in such case, the brine pH is lower than 9. On the other hand, the presence of calcite may lead to higher pH than 9. If we are unable to calculate the resulting brine composition for higher $P_{CO_2(g)}$, we will use the composition presented in Table 17. Therefore, this task has two goals – first, to determine the relevant brine compositions via calculation, and second, to develop a method to synthesize the aforementioned brines. We will perform experiment in presence and in absence of organic ligands (acetate, citrate, EDTA, and oxalate). The concentration of organic ligands to be used is yet to be determined; we will probably use larger concentrations than indicated by the code calculations to compare to the results obtained without ligands. If we determine that organic ligands influence the system, we will study the influence of a variation of ligand concentrations.

9.2.2 Task 2: Construction and Validation of a Mixed Flowing Gas Exposure System

In order to perform the atmospheric and aqueous experiments needed to assess the tendency for Fe and Pb to form carbonates in the WIPP following room closure, a system capable of maintaining the applicable environmental conditions (see Section 9.1.2) must be assembled. The system described below will enable this environment to be accurately achieved and reliably maintained throughout the course of this testing.

The system itself can be broken down into three general parts – the gas supply subsystem, the gas mixing and exposure chambers, and the gas analysis subsystems. The following paragraphs detail each of the aforementioned subsystems.

In order to assure that the purity of the gas supply is maintained within acceptable limits, gas will be delivered from a series of compressed gas tanks supplied by an appropriate vendor. Tanks will be manifolded together as needed to provide the desired flow rates. There will be two source gas streams in this study – the first being the dry gas stream, and the second being a humid gas stream. The gas distribution system itself is illustrated in Figures 2 and 3. As indicated in the figures, each of the gas streams will be passed through an O_2 getter prior to delivery to the exposure chamber, ensuring that the O_2 content is maintained below 50 ppb.¹ Gas for both streams will be drawn from the supply tanks through mechanical flow regulating valves which ensure that the flow rate remains constant independent of the supply pressure (thus the supply pressure will not deviate as the supply tanks are depleted and decrease in pressure). The

¹ The source gas for the exposure system will be effectively 100% nitrogen (with appropriate additions of CO_2 and/or H_2S). As such, the gas stream will likely be sufficiently oxygen free so as to not require the use of getters during normal operation. However, during gas tank changes or other disturbances to the gas delivery system, air (and thus oxygen) may be introduced into the gas stream. In order to compensate for this effect, along with any trace oxygen contamination of the nitrogen source gas, oxygen scavengers have been added to the gas supply stream.

actual flow rates will be continuously monitored and logged via mass flow meters. Since the target humidity level within the test environment is 70%, 70% of the total gas flow sent to the exposure chamber will be in the form of N_2 which has been humidified to 100% relative humidity (which will later be mixed with the remaining 30% of the gas stream which will be dry). Humidification will be accomplished through the use of a simple saturator – the dry N_2 gas will be passed through a dispersion system and bubbled through warm (40°C) deionized water where it becomes saturated with moisture (at this point, the gas stream will be 40°C and 100% relative humidity). Once it has been through the humidifier, the gas will be passed into a condenser (similar in concept to the saturator) which is at the target temperature of 30°C. At this point, the gas will be brought to the target temperature and any liquid moisture will be removed from the gas stream. Once the humidified gas stream has passed through the condenser, it will be sent to the main mixing chamber prior to passing into the exposure chamber (described below).

The second leg of the gas delivery system consists of the dry contaminant stream. Here again mechanical flow regulators will be used to ensure a constant delivery rate of gas – in this case, both CO_2 (or a CO_2/N_2 mixture) and dry N_2 will be utilized. The flow from both gas streams will be monitored with mass flow meters, and the flow rates logged as a function of time. The N_2 and CO_2 containing dry gas streams will then pass into a mixing chamber, after which they will be delivered to the temperature control chamber, where they will be mixed with the 100% relative humidity N_2 gas stream discussed above. The flow rate of the CO_2 stream will be set such that the desired CO_2 level is achieved within the exposure chamber.

The humid and dry gas streams described above will both flow into a second mixing chamber where they will mix and be brought to the desired temperature. After passing through the mixing chamber, the gas stream, now at the desired humidity and CO_2 concentration, will be delivered to the exposure chamber, which it will flow through, as illustrated in Figure 2. The exposure chamber will be located (along with the condenser and second gas mixing chambers described above) within a temperature controlled incubator. The temperature control system will be selected such that the temperature within the system is maintained irrespective of the external environment (i.e., the system should be capable of heating and cooling). The exposure chamber itself will be sized such that all of the proposed experiments (described below) can be housed within it. In addition, electrical and mechanical feed-throughs will be incorporated such that periodic removal of specimens, performance of rudimentary electrochemical experiments, and sampling of brine compositions can be performed.

In order to allow exposure to gas streams in addition to CO_2 – in this case, H_2S , another leg must be added to the gas delivery system. This is illustrated schematically in Figure 3. An additional flow control valve will be added which will deliver dry N_2 to a permeation device. The permeation device (permeation tube) is a device which emits a desired specie at a known rate. The permeation device will be placed inside a glass chamber which is held at a constant temperature. The N_2 flow rate into the permeation device chamber will be selected such that the gas concentration exiting the permeation chamber is at the desired level. A flow controller and vent valve combination will then be used to regulate the delivery of the contaminant specie to the dry gas mixing chamber described previously. The gas flows to each of the four reactors are illustrated schematically in Figure 4.

The final portion of the atmospheric corrosion system is the gas analysis segment, shown schematically in Figure 5. Compositional analysis will be performed on the exit stream from the reaction chamber to ensure that the desired concentration is maintained. As the aggressive species are more likely to be depleted/consumed in the reaction chamber, it is highly desirable that the concentration be monitored real-time, rather than periodically. The gas stream will be analyzed for the relative humidity, CO₂, and H₂S level. This may be accomplished utilizing commercially available analyzers capable of detecting H₂S in the low ppb and CO₂ in the low ppm concentration ranges (such devices have been successfully applied to atmospheric corrosion systems commonly used at Sandia in the Corrosion and Electrochemical Science Dept.). In order to minimize the number of detectors required, a series of solenoid valves coupled with control hardware and software (described below) will be used to enable periodic sampling of each gas stream, as illustrated in Figure 5.

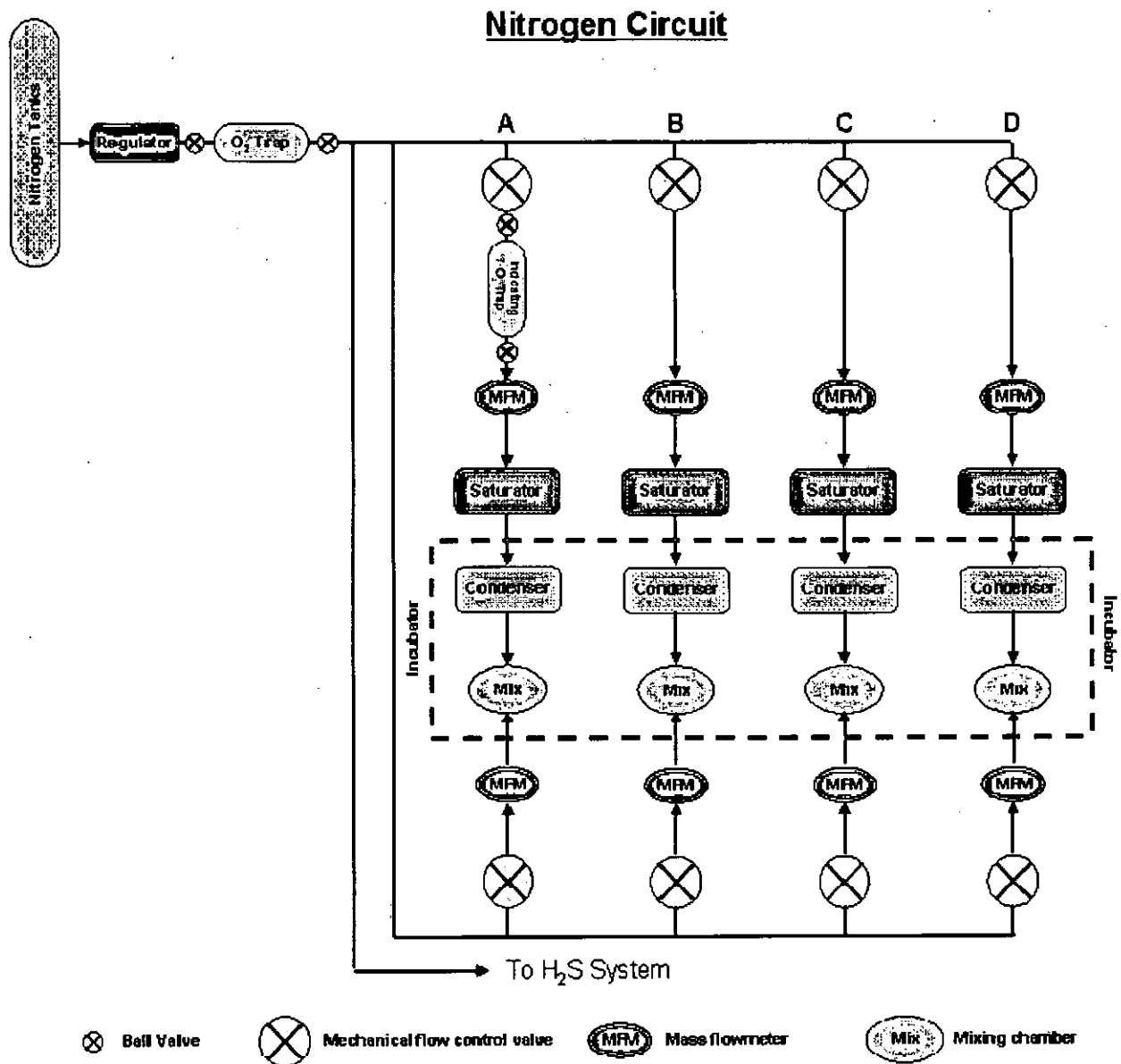


Figure 2. N₂ gas circuit for the gas exposure system. This circuit includes the wet N₂ streams (top portion) as well as the dry N₂ streams. Also shown are two O₂ traps – a large capacity trap in the main supply line, and an indicating trap in one of the wet supply lines.

Carbon Dioxide and Hydrogen Sulfide Circuits

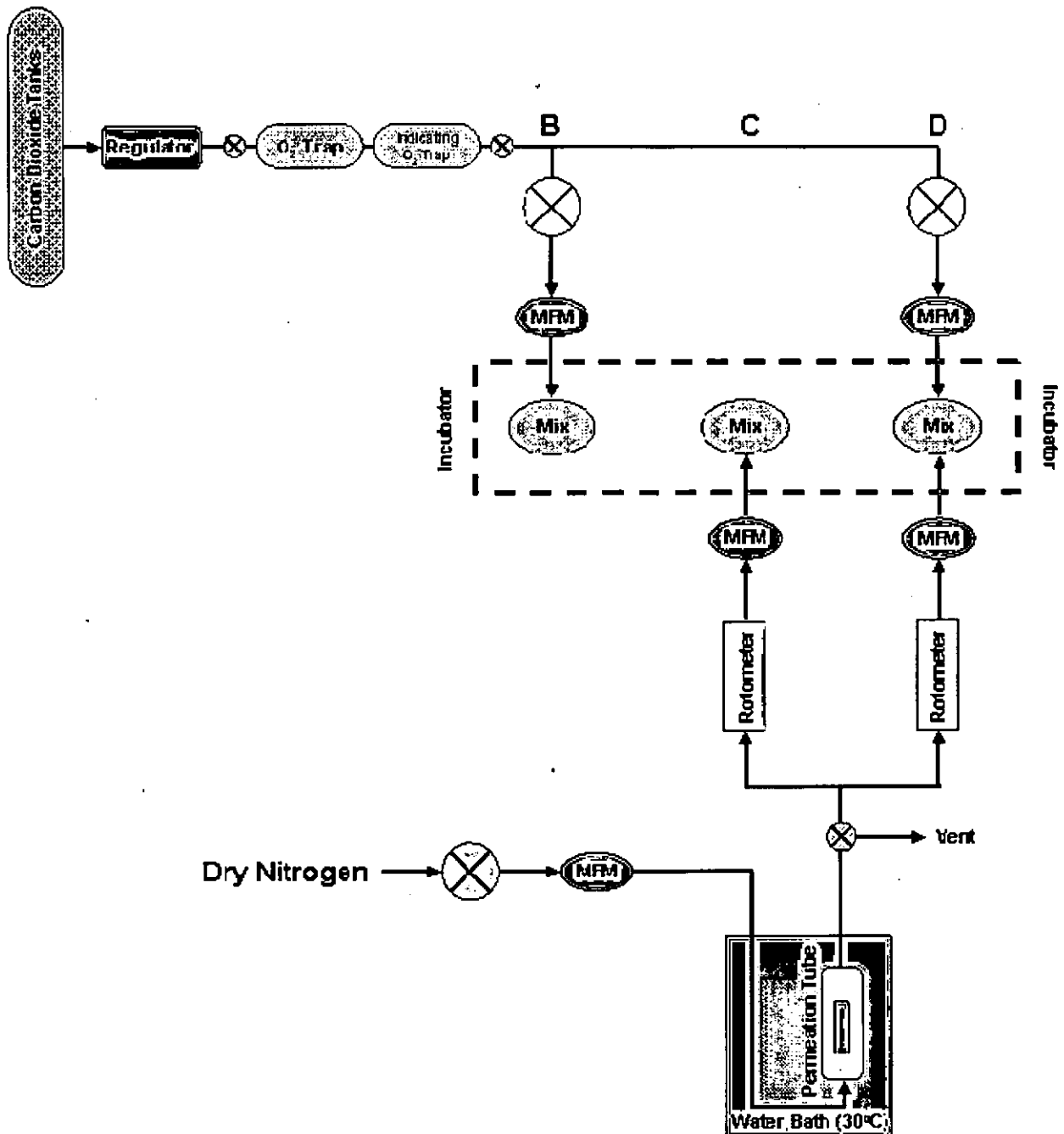


Figure 3. Contaminant gas streams for the gas exposure system. Upper portion of the figure illustrates the CO₂ supply (equipped with O₂ traps similar to those described above). The lower portion illustrates the H₂S gas supply system – note that the supply gas for this leg is dry N₂ and as illustrated in Figure 2.

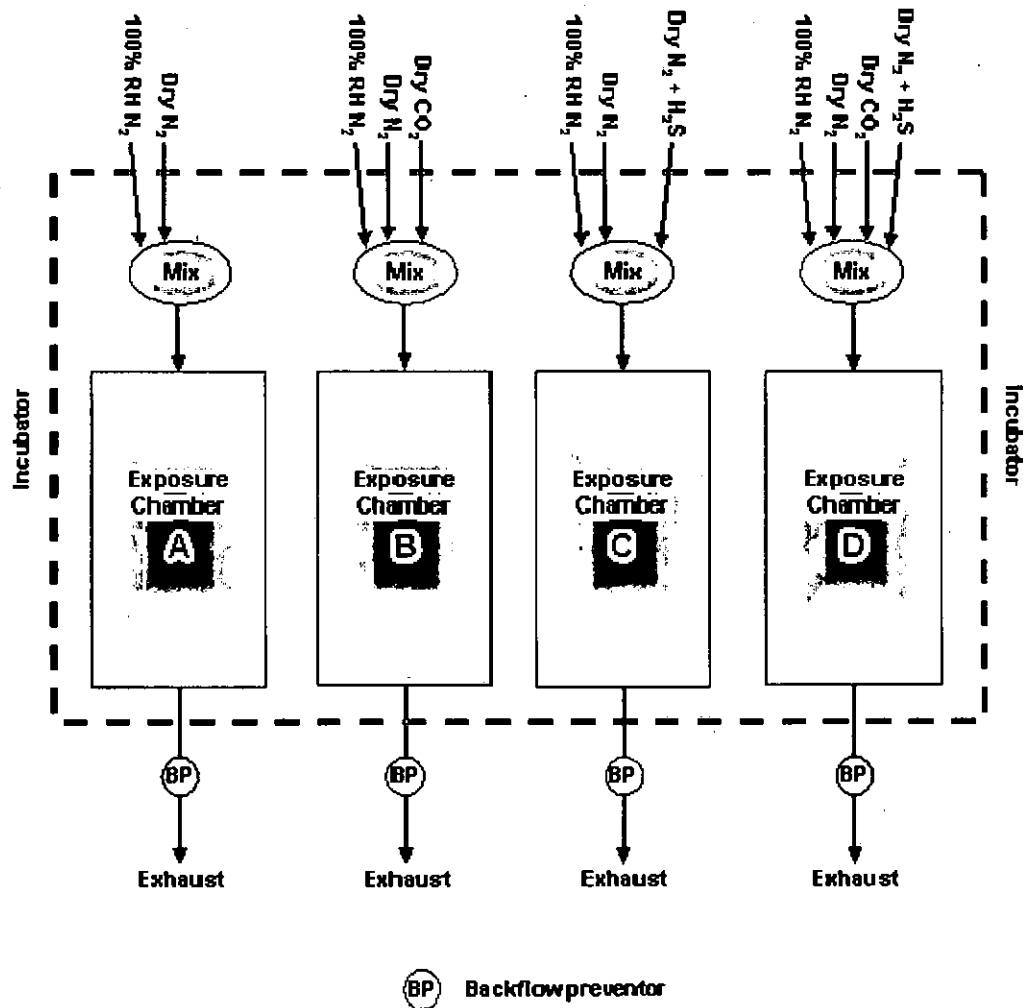


Figure 4. Schematic representation of the gas flow streams passing into each of the four exposure chambers.

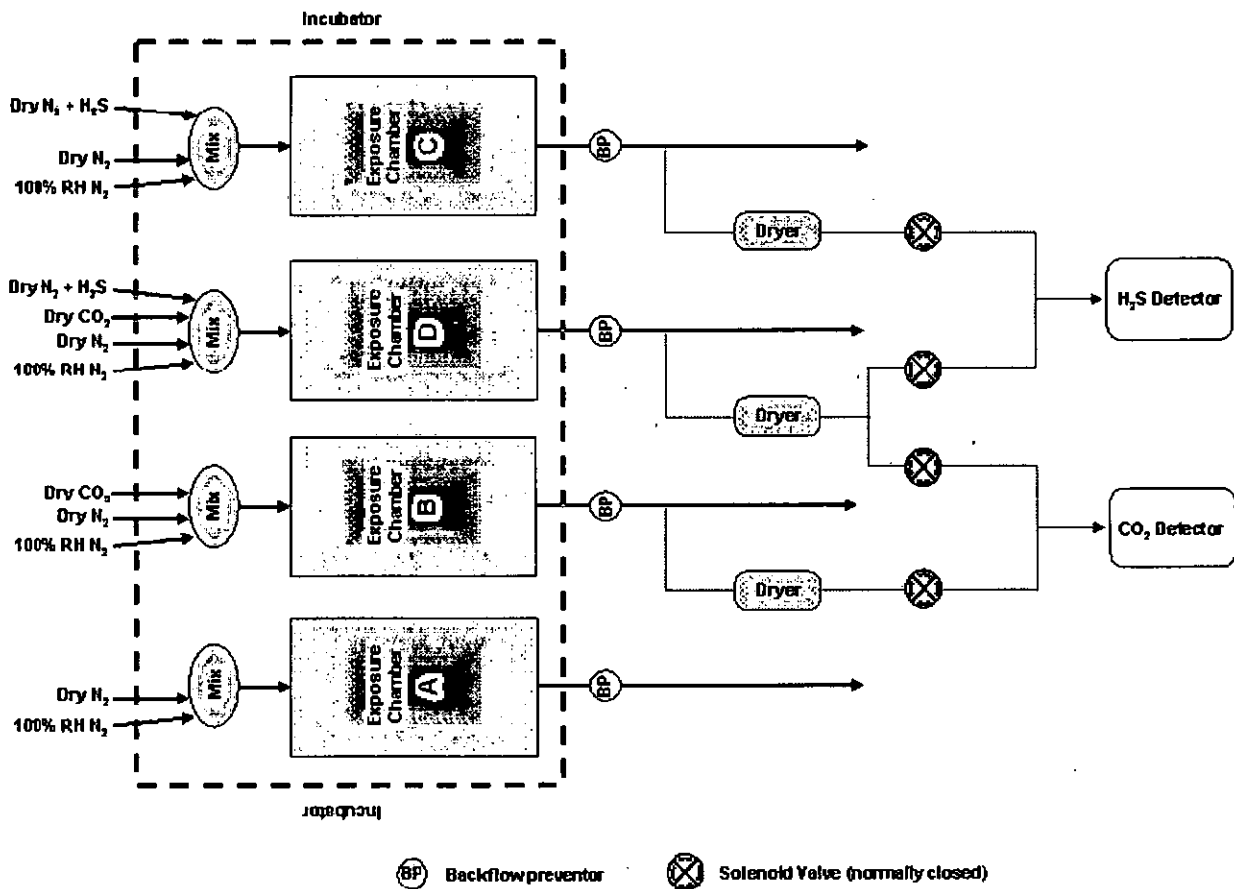


Figure 5. Schematic representation of the gas composition analysis system. This system consists of a series of perma-pure gas dryers, a gas manifold (controlled by solenoid valves) to route the gas to each analyzer, and the two gas analyzers themselves.

9.2.3 Task 3: Software Qualification - Monitoring System and Software for the Mixed Flowing Gas Exposure System

In this task, the data acquisition system and software will be constructed to monitor the mixed flowing gas system defined in the previous task. The procedures defined in NP 19-1 will be followed, and the required documentation generated. The text below summarizes the system and software requirements.

9.2.3.1 PURPOSE

This system will continuously monitor the gas flow rates and compositions throughout the course of the experiment. Warning notices will be incorporated to notify the user of any adjustments which are required to address any deviations from the desired gas composition. Note that the purpose of the system is to monitor only – all flow control will be accomplished through mechanical valving.

9.2.3.2 FORMAT

The data acquisition system will consist of the following components (all National Instruments hardware):

- SCXI-1000 4 slot chassis (system backbone)
- SCXI-1600 Data acquisition and control module
- SCXI-1112 8 channel thermocouple module
- SCXI-1100 32 channel multiplexer amplifier
- SCXI-1124 6 channel isolated DAC module

The data acquisition software will be a routine written in National Instruments LabVIEW – this software will be utilized to monitor mass flowmeters, monitor thermocouples, actuate solenoid valves for the gas sampling system, and acquire data from the gas analysis hardware. The QA process for the software will be conducted in accordance with the procedures defined in NP 19-1.

9.2.3.3 DETAILED TEST SYSTEM DESCRIPTION

In simple terms, there are four portions of the gas exposure system (described in section 9.2.2) – the gas supply, the humidity source, the exposure chamber, and the compositional analysis systems.

The gas source will consist of either pressurized tanks or an appropriate gas generator which supplies high purity N₂ or CO₂ gas (potentially at a range of pressures) to a series of mechanical flow valves. The flow valves route the gas to the other components of the system. The output from each mechanical flow valve is monitored by a mass flow meter, which will in turn be monitored by the software package described here.

The humidity source will take a dry gas stream and increase its humidity to 100%. This is accomplished by passing the gas through a saturator which is essentially a warm bath of deionized water (at a temperature greater than the exposure chamber temperature), then into a condenser which is at the same temperature as the exposure chamber, then finally into the test

chamber itself. In addition to the flow rates described above, the system will also monitor the temperature within each saturator, providing a warning indicator if the temperature drifts outside the acceptable temperature range, signaling the operator to make appropriate adjustments.

The composition analysis system has two subcomponents – the first are the composition analyzers themselves (for CO₂ and H₂S), and the second is a series of solenoid valves which route the gas streams from the exposure chambers to the appropriate detector. The software package will control the solenoid valves (see Figure 5 above) and route the gas stream to the appropriate detector, and acquire data from the detector.

The flow rates (from the flowmeters), temperatures in the saturators and exposure chamber (via thermocouples), and the composition of each gas stream will be monitored and recorded. Simple calculations will be performed to determine the anticipated supply gas compositions based upon measurements taken from the flowmeters. These values will be recorded and then compared to the measured gas composition. Should the two deviate from one another by an unacceptable amount (+/- 15% or 3ppb, whichever is greater, as defined in ASTM B827 (ASTM, 2003a)), a warning message will be displayed indicating that the user must appropriately document the deviation, then manually adjust the supply flows to reach the desired test conditions.

9.2.3.4 PROGRAM PROCESSES/ACTIONS:

1. Monitor flow meters
 - a. Display flow rates on computer screen
 - b. Log data to an excel spreadsheet at a user defined time interval
 - c. Display warning/caution indicator if flows drift out of range
 - d. Present a calculated gas composition based upon flow rates
2. Monitor system temperatures
 - a. Display temperatures on computer screen
 - b. Log data to an excel spreadsheet at a user defined time interval
 - c. Display warning/caution indicator if any temperatures drift out of range
3. Monitor gas chemistry
 - a. Control solenoid valves in multiplexing system to select which gas stream is to be analyzed
 - b. Display measured concentrations on the computer screen
 - c. Log the measured and calculated concentrations of each component to a spreadsheet at a user defined time interval
 - d. Display a warning/caution indicator if the concentrations deviate more than a user defined percentage from the calculated inlet concentrations

9.2.3.5 VERIFICATION OF SOFTWARE FUNCTIONALITY

1. Apply series of known flow rates to each flow meter over a period of time and verify that the data acquisition system properly measures and records the data.

2. Apply series of known temperatures to each thermocouple over a period of time and verify that the data acquisition system properly measures and records the data.
3. Apply a temperature outside the predefined operating window and verify that the system warns the user and then responds properly when the correct parameters are re-established.
4. Verify that the system is able to cycle through the valves and supply a sample gas stream to each composition analyzer from each chamber which it is monitoring.
5. Apply gas of a known composition to each analyzer and verify that the system is able to correctly measure and record the data.
6. Apply gas of a known composition to the system which is outside the predefined operating window to verify that the system warns the user and then responds properly when gas of the proper concentration is supplied.
7. Allow system to run for an extended time period to verify that the code is stable.

9.2.4 Task 4: Evaluation of Carbonation of Fe in WIPP Internal Atmosphere and Likely Equilibrium Brines

Once the exposure system has been constructed and appropriate sample geometries identified, the long term experiments may be initiated. The goal of this task is to determine the tendency of the Fe-based alloys used to construct the drums utilized within the WIPP to consume CO₂ from the in-room environment through the formation of iron carbonates. Coupons will be made from material similar in composition to that found within the WIPP. Samples will be evaluated in three conditions – totally immersed within the brine, partially immersed within the brine, and suspended above the brine. A series of experiments will be performed in parallel for each of the brines defined in Task 1 above.

In addition to the primary corrosion coupons, a series of instrumented samples will be included such that the corrosion rate may be assessed as a function of time. The samples will include a set of three electrodes – a platinum wire (counter electrode), a chloridized silver wire (reference electrode) and a sample of the desired material – electrochemical impedance spectroscopy will be performed to assess the state of the surface as a function of time.

During the course of the experiment, samples will be periodically removed and the corrosion product analyzed to determine the extent of corrosion which has taken place, and assess the quantity of carbonate which has formed (and hence, CO₂ consumed). At a minimum, one set of samples will be removed in the middle of the test (approximately 1 year) and a second set upon completion of the test (approximately 2 years). Note that once removed from the system, samples will not be reintroduced (i.e., once a sample is out, it will stay out). In addition, brine samples will be periodically taken to establish to what degree the solution composition has been altered by the corrosion process. (It should be noted that samples from the bulk brine will not necessarily be indicative of the solution composition which exists at the metal solution interface within the corrosion product layer.) For all corrosion coupons removed from the system, the composition and quantity of corrosion product will be identified. In addition, a weight loss measurement will be taken and converted to an average dissolution rate. Finally, the metal surface will be photodocumented (both before and after the corrosion product has been removed).

9.2.5 Task 5: Evaluation of Carbonation of Pb in WIPP Internal Atmosphere and Likely Equilibrium Brines

The goal of this task is to determine the tendency of the Pb liners within some of the drums utilized within the WIPP to consume CO₂ from the in-room environment through the formation of lead carbonates. Two forms of samples will be evaluated – single Pb coupons compositionally similar to the actual Pb liners, and Pb-Fe galvanic couples (simulating the geometry which exists within the Pb lined drum). These samples will be evaluated in three conditions – totally immersed within the brine, partially immersed within the brine, and suspended above the brine. A series of experiments will be performed in parallel for each of the brines defined in task 1 above. Experiments will be performed following the procedures defined in ASTM G1 (ASTM, 2003b).

In addition to the primary corrosion coupons, a series of instrumented samples will be included such that the corrosion rate may be assessed as a function of time. The samples will include a set of three electrodes – a platinum wire (counter electrode), a chloridized silver wire (or other similar reference electrode) and a sample of the desired material – electrochemical impedance spectroscopy will be performed to assess the state of the surface as a function of time.

During the course of the experiment, samples will be periodically removed and the corrosion product analyzed to determine the extent of corrosion which has taken place, and assess the quantity of carbonate which has formed (and hence, CO₂ consumed). At a minimum, one set of samples will be removed in the middle of the test (approximately 1 year) and a second set upon completion of the test (approximately 2 years). Note that once removed from the system, samples will not be reintroduced (i.e., once a sample is out, it will stay out). In addition, brine samples will be periodically taken to establish to what degree the solution composition has been altered by the corrosion process. (It should be noted that samples from the bulk brine will not necessarily be indicative of the solution composition which exists at the metal solution interface within the corrosion product layer.) For all corrosion coupons removed from the system, the composition and quantity of corrosion product will be identified. In addition, a weight loss measurement will be taken and converted to an average dissolution rate. Finally, the metal surface will be photodocumented (both before and after the corrosion product has been removed).

9.3 Test Matrix

9.3.1 General Environmental Parameters

Temperature: 28°C

Basis: Temperature measurements made within WIPP Room H (Munson, 1987)

Relative Humidity: 72%

Basis: Based upon the FMT calculations performed by Brush (Brush, 2005), the anticipated relative humidities in the headspace over each of the brines being evaluated in this study are effectively equivalent. As such, all of the brines for a given atmospheric condition will be held within the same mixed flowing gas chamber.

9.3.2 Materials to be Evaluated

Iron: ASTM A1008 and ASTM A36 carbon steels

Basis: The majority of the containers within the WIPP are drums of various sizes, all of which are constructed of ASTM A1008 compliant material. The second most prevalent Fe alloy is ASTM A36 carbon steel which is used in the large boxes, 10 drum overpacks, etc.

Lead: chemical-copper lead (UNS L51121)

Basis: While the Pb alloy used within the RH waste containers is not specifically called out, this grade is the one commonly used for chemical processing, corrosion performance, etc. (QQ-L-171e grade C)

9.3.3 Atmosphere

Atmosphere 1: N₂

Atmosphere 2: N₂ + CO₂

Atmosphere 3: N₂ + H₂S

Atmosphere 4: N₂ + CO₂ + H₂S

Basis: As discussed above, the predicted atmosphere within the WIPP resulting from microbial consumption of the CPR materials in the waste will be a combination of inert (e.g., CH₄) and active (e.g., CO₂ and H₂S) gasses. In these experiments, N₂ will be substituted for CH₄ as the inert carrier gas to ease ES&H concerns, with both CO₂ and H₂S as potentially aggressive species.

9.3.4 Brine Compositions

Chemistry 1: ERDA-6 (Synthetic Castile Formation brine)

Chemistry 2: GWB (Synthetic Salado Formation brine)

Basis: These two brines are the predicted compositions which will come into contact with the waste over time.

Chemistry 3: ERDA-6 after equilibration with Periclase, halite, and anhydride

Chemistry 4: GWB after equilibration with Periclase, halite, and anhydride

Basis: Equilibration of the two anticipated brine chemistries with the engineered barrier.

Organic Ligands (EDTA, Oxalate, Acetate, and Citrate)

Chemistry 5: Chemistry 1 + Organic Ligands

Chemistry 6: Chemistry 2 + Organic Ligands

Chemistry 7: Chemistry 3 + Organic Ligands

Chemistry 8: Chemistry 4 + Organic Ligands

Basis: Organic ligands, while typically omitted from WIPP exposure experiments, have been found to impact the electrochemical behavior of both Fe and Pb alloys. As such, all four of the previously defined brine chemistries will also be evaluated with the organic ligands present.

9.3.5 Sample Positioning

Atmospheric (exposed only to atmosphere)

Partially Inundated (located at waterline)

Inundated (submerged within brine under atmosphere)

Basis: Due to the limited quantity of brine which is predicted to permeate into the waste, it is reasonable to assume that not all of the material will come into contact with liquid brine. As such, all three materials identified above will be evaluated while inundated with brine, while exposed only to the humid atmosphere which will exist above the brine, and while partially immersed in the brine (half below the surface of the brine, half above it). In the latter case, care will be taken to insure that the samples are not subject to splashing from the brines. Furthermore, care will be taken to minimize any sample stirring to avoid disturbing the corrosion product layers or altering the distribution of locally depleted species. Partially immersed samples have been added to the test matrix in an effort to more thoroughly explore the waterline results observed by Telander and Westerman (Telander and Westerman, 1993; 1997) where the nature and chemical composition of the corrosion product differed from regions away from the waterline. Furthermore, as the material within the WIPP will likely not be completely immersed in brine, these tests will broaden our understanding of the corrosion processes and products likely to be present.

9.3.6 Experimental design

Each of the alloys described above will be exposed to the four brines in each of the four atmospheres. Due to the similar humidity which would result at equilibrium over each brine, all four brines will be evaluated simultaneously in each atmosphere, necessitating the four chamber system described in Section 9.2.2. As such, within each chamber there will be:

- Samples of each material (minimum of three replicates) suspended in the atmosphere, away from the vessels containing brine
- Samples (minimum of three replicates) of each material in each of the four brines

10 SAMPLE CONTROL – DATA QUALITY CONTROL

10.1 Sample Control

The sample control for the work under this Test Plan will follow NP 13-1. Each sample will be appropriately labeled. Sample preparation, utilization, and final disposition will be documented. When samples are not in the possession of individuals designated as responsible for their custody, they shall be stored in a secure area with associated documentation (e.g. SNL WIPP Activity/Project Specific Procedure (SP) Form SP 13-1-1, "Chain of Custody").

10.2 Data Acquisition Plan

Data collection procedures are specific to individual instruments. For details of the data acquisition for a particular instrument, see the SP or Users Manual for that instrument. Any data acquired by a data acquisition system (DAS) will be attached directly to the Scientific Notebook or compiled in separate loose leaf binders with identifying labels to allow cross reference to the appropriate Scientific Notebook, as indicated in the Scientific Notebooks Procedure NP 20-2. If the instrument allows data to be recorded electronically, copies of the data disks will be submitted to the Waste Isolation Pilot Plant (WIPP) Records Center according to NP 17-1 "Records." If possible, data files may be transferred to an electronic storage device (e.g. ZIP disks or CD ROM) for submittal to the records center. For instruments that do not have direct data printout, the instrument readings will be recorded directly into the scientific notebook or in a separate loose leaf binders (scientific notebook supplements per NP 20-2) with identifying labels to allow cross reference to the appropriate Scientific Notebook, as indicated in the Scientific Notebooks Procedure NP 20-2. Current versions of the DAS software will be included in the SNL WIPP Baseline Software List, as appropriate.

Quality control of the Scientific Notebooks will be established by procedures described in NP 20-2 "Scientific Notebooks." Methods for justification, evaluation, approval, and documentation of deviation from test standards and establishment of special prepared test procedures will be documented in the Scientific Notebooks. Procedures including use of replicates, spikes, split samples, control charts, blanks and reagent controls will be determined during the development of experimental techniques.

The numerical data will be transferred from data printouts, electronic media, and scientific notebooks to Microsoft Excel (Office 2003 version or later) spreadsheets. Data transfer and reduction shall be performed in such a way to ensure that data transfer is accurate, that no information is lost in the transfer, and that the input is completely recoverable. A copy of each spreadsheet will be taped into the scientific notebook.

10.3 Data Identification and Use

All calculations performed as part of the activities of this test plan will be documented in scientific notebooks. The content and organization shall follow the Scientific Notebook Procedure NP 20-2. The notebooks will be reviewed periodically for technical and QA content and adequacy, as explained in the Scientific Notebook Procedure NP 20-2.

11 EQUIPMENT

11.1 Measuring and Test Equipment (M&TE)

A calibration program will be implemented for the work described in this test plan in accordance with NP 12-1, "Control of Measuring and Test Equipment." This M&TE calibration program will meet the requirements in procedure NP 12-1 for: (1) receiving and testing M&TE; (2) technical operating procedures for M&TE; (3) the traceability of standards to nationally recognized standards such as those from the National Institute of Standards and Technology; (4) maintaining calibration records. In addition, NP 13-1 (Control of Samples and Standards) and SP 13-1 (Chain of Custody) identify requirements and appropriate forms for documenting and tracking sample possession. The spread-sheet and other computer based data handling will follow NP 9-1 (Analyses).

A variety of measuring and analytical equipment will be used for the work described in this test plan. This equipment includes that listed below, as well as equipment not yet purchased. A complete equipment list, including serial numbers, will be maintained in the scientific notebooks.

11.2 Weighing Equipment

Several balances may be used for this project. These include a Mettler AT-261 five-decimal place electronic balance, an ANC three-decimal place balance, and top loading balances and scales with maximum ranges of 2 to 30 kg. Balance calibration checks will be performed daily or prior to use (whichever is less frequent) using NBS-traceable weight sets, which, in turn, are calibrated by the SNL Mechanical Calibration Laboratory every two years. The balance calibration will be performed according to the procedure SP 12-1 (Use of Laboratory Balances and Scales). Balance calibration checks will be recorded in the current Balance Logbook, and a note indicating the page number of the calibration check and other pertinent information will be made within the appropriate Scientific Notebook.

11.3 Temperature Measuring Equipment

Mercury thermometers are used in the facility. A calibration check of these thermometers is performed annually against an ERTCO High Precision digital thermometer (model 4400), which is itself calibrated by the SNL Primary Standards Laboratory every year. The results of these calibration checks are recorded in the current Thermometer Logbook.

11.4 Liquid Measuring Equipment

Standard Laboratory Class A glassware (pipettes, volumetric flasks, etc.) will be used at all times. In addition, several adjustable Eppendorf pipettes are available for use in the laboratory. The calibration of pipettes will be checked routinely against a calibrated balance, and the results documented in the appropriate scientific notebook.

11.5 Other Analytical Equipment

11.5.1 Ovens and Furnace

Six Precision Telco Lab ovens are being used to hold samples at elevated temperatures. Temperature is monitored, maintained, and recorded on a daily schedule in the Oven Temperature logbook. A Fisher Isotemp furnace is used to determine Loss on Ignition (LOI).

11.5.2 pH Meters and Autotitrators

Solution pH may be measured using pH meters and/or autotitrators. A Mettler Model MA235 pH/Ion Analyzer and a Mettler Model DL25 Autotitrator will be used for this purpose. The range for all pH meters is 0.00 to 14.00. Electrodes will be calibrated before each use or daily (whichever is less frequent) with pH 4, 7, and/or 10 buffers manufactured by Fisher Scientific with unique lot numbers and expiration dates; traceable to the National Institute of Standards and Technology (NIST). The accuracy of the buffers is ± 0.01 pH units; buffer values will be adjusted for laboratory temperatures as per buffer instruction sheets if necessary. Calibration checks will be recorded in the scientific notebook. Measuring pH in concentrated brines is difficult, and a procedure will be developed to calibrate pH meters. The pH meters will be used according to the procedure SP 12-14 (Use of pH Meters and Electrodes). There is currently no procedure describing the use of the Mettler Model MA235 pH/Ion Analyzer and the Mettler Model DL25 Autotitrator. If this equipment is used, a procedure will be produced. Until that time, detailed procedure descriptions based on the instrument manual will be documented in laboratory notebooks.

11.5.3 Equipment for Chemical Analysis

Three instruments may be used for chemical analyses. The first is a Perkin Elmer Optima 3300 DV inductively-coupled plasma optical emission spectrometer (ICP-OES); the second is a Cary 300 UV-Visible Spectrophotometer; and the third, is a UIC, Inc. Carbon Analyzer, consisting of an acidification module, a furnace module, and a CO₂ coulometer. These instruments will be user-calibrated each time they are used and documented in their respective Logbook and in the scientific notebooks. The Carbon Analyzer will be used according to the procedure SP 12-2 (Use and Maintenance of the UCI, Inc. Model CM5014 CO₂ Coulometer, CM5130 Acidification Module and CM5120 Furnace Apparatus). If the two other pieces of equipment are used in this work, procedures will be generated. Until that time, detailed procedure descriptions based on the instrument manual will be documented in laboratory notebooks.

11.5.4 Equipment for Mineralogical, and Textural Characterization

The mineralogy and texture may be characterized using either an Olympus BX60 Polarizing Microscope or a JEOL JSM 5900LV scanning electron microscope (SEM). Calibration standards will be used to verify instrument magnification when these instruments are used. Bulk sample mineralogy will be determined using a Bruker AXS D-8 Advance X-Ray Diffractometer (XRD). A mineral standard will be run periodically to verify diffraction line

positions. Calibration results will be documented in the instrument Logbooks and the scientific notebooks. If these instruments are used in this work, procedures will be generated. Until that time, detailed procedure descriptions based on the instrument manual will be documented in laboratory notebooks.

Information Only

12 TRAINING

All personnel involved in the experiments described in this Test Plan will be trained and qualified for their assigned work. This requirement will be implemented through NP 2-1, "Qualification and Training." Evidence of training to assigned NPs, SPs, TOPs, this test plan, ES&H procedures, and any other required training will be documented through Form NP 2-1-1 Qualification and Training. Annual Refresher QA training will ensure on-site personnel are trained to the WIPP QA Program. Specifically, the following NPs and SPs are applicable:

- NP 2-1 – "Qualification and Training"
- NP 6-1 – "Document Review Process"
- NP 9-1 – "Analyses"
- NP 12-1 – "Control of Measuring and Test Equipment"
- NP 13-1 – "Control of Sample and Standards"
- NP 17-1 – "Records"
- NP 20-2 – "Scientific Notebooks"
- SP 13-1 – "Chain of Custody"
- SP473548 – "ES&H Standard Operating Procedure, Activities in the Sandia National Laboratories/Carlsbad Laboratory, Building NPHB (U)."

13 HEALTH AND SAFETY

The work proposed in this test plan will be performed in the Sandia National Laboratories – Carlsbad Program Group laboratory and will conform with SNL ES&H and follow the ES&H Standard Operating Procedure (SOP) SP473548 (Wall, 2005), or the most current version. The hazards associated with the experiments proposed in this test plan can be broken down into three areas – electrical, chemical, and thermal. The concerns and mitigation strategies for each of these areas are described below.

13.1 Electrical

As with most active systems, there will be numerous leads run from power supplies and other electrical equipment in order to operate the experiments. All of the wiring will be covered/shielded such that there are no exposed, energized wires during normal operation of the system. All the electrical outlets will be grounded, and those within 6 feet of water sources are ground-fault-interrupt (GFI) protected. Some analytical instruments have built-in power supplies, generating voltages up to 60 kV (XRD). The power supply design prevents exposure of the users to an electrical hazard. No direct contact with energized circuits greater than 50 volts is expected to be encountered during the operation of this experiment.

13.2 Chemical

13.2.1 General Chemical Compounds

There are a number of chemical hazards associated with the experimentation described in this document. The hazards associated with each chemical are found in the MSDS files, which are kept in the laboratory.

The brines used during this experimentation are not a direct hazard for those performing the experimentation. But the disposal of the brines will be handled as part of the hazardous wastes stream, in accordance with the governing discharge into the Carlsbad sanitary sewer system, as currently described in the laboratory SOP (Wall, 2005), or the most current version. Secondary containment will be used to minimize the potential for unintended release of the brine in the chambers and benches.

13.2.2 Inert Gases

The work will involve the large quantities of inert gases (nitrogen and carbon dioxide) which will be used for the bulk of the exposure environment. The danger associated with these gases is exclusion of oxygen from the work area. While the risk is small due to the low flow rates involved (less than 4000 sccm (standard cubic centimeters per minute (i.e., milliliters per minute)) during normal operation), there could be unforeseen circumstances which lead to the release of larger quantities. In order to mitigate this hazard, oxygen level monitors as well as local ventilation will be utilized.

If one or several O₂ alarms are triggered, stay out of the area until the alarm shut off. If the alarm does not shut off the facility manager and laboratory manager shall be notified.

13.2.3 Hydrogen Sulfide

13.2.3.1 HAZARDS OF H₂S AND REGULATION

This section is not intended to replace the information provided by the H₂S material safety data sheet (MSDS); it merely highlights important information regarding H₂S(g). The reader is strongly encouraged to read the most recent H₂S MSDS.

H₂S(g) which will be used in several of the exposure chambers of this work. H₂S(g) is a colorless, highly toxic, flammable gas that is responsible for the foul odor of rotten eggs. This gas is slightly heavier than air, so it tends to concentrate at the bottom of poorly ventilated spaces. H₂S is considered highly toxic because it can poison different body systems; comparable to the effect of hydrogen cyanide, it blocks oxygen and stops cellular respiration. Additionally, H₂S can be difficult to detect without a proper alarm system, because its breathing may temporarily paralyze the olfactory nerve making it impossible to smell the gas after an initial strong exposure. In case of poisoning, several treatments can be applied, among which the immediate inhalation of amyl nitrite or of pure oxygen. Table 18 presents the symptoms observed after the exposure to different H₂S(g) concentrations.

Table 18. Symptoms Observed after Different H₂S Exposure

H ₂ S concentration exposure	Symptoms
0.0047 ppm	Recognition threshold; 50% of humans can detect the characteristic rotten egg odor of hydrogen sulfide
10 – 20 ppm	Slight eye irritation
50 – 100 ppm	Eye damage
150 – 250 ppm	Olfactory nerve paralyzed after few inhalations; Sense of smell disappears
320 – 530 ppm	Pulmonary edema; Possible death
530 – 1000 ppm	Loss of breathing
800 ppm	Lethal concentration for 50% of humans after 5 minutes exposure (LC50)
> 1000 ppm	Immediate collapse after one breath

A variety of H₂S exposure limits have been established, from a Threshold Limit Value (TVL) of 10 ppm, as defined by the American Conference of Governmental Industrial Hygienists (ACGIH), to a PEL of 20 ppm, as defined from the Occupational Safety and Health Administration (OSHA) (ceiling).

H₂S(g) is also highly flammable, forming an explosive mixture with air, in concentration from 4.0 % (40,000 ppm) to 46 % (460,000 ppm). H₂S autoignites in the presence of oxygen at 260 °C.

13.2.3.2 SAFETY IMPLEMENTATION

A number of steps will be taken to minimize the hazards associated with this material. First, the gas will be supplied via a permeation device, rather than as a tank of compressed gas. This dramatically reduces the total quantity of the gas present in the laboratory, as well as limiting its release rate. The permeation device releases H₂S(g) at a known rate (usually expressed in ng/min); H₂S(g) flows at a known rate across the chamber containing the permeation tube, which in turn generates a gas stream of known H₂S(g) concentration. The gas

stream is diluted with a dry gas feed into the chamber in order to achieve the desired concentration.

In addition, the concentrations of hydrogen sulfide in the exposure chambers will be kept below 10 ppm (the current OSHA PEL is 20 ppm (ceiling) and the ACGIH TVL is 10 ppm). The $\text{H}_2\text{S}(\text{g})$ partial pressures applied to a system depends on the $\text{CO}_2(\text{g})$ partial pressures used. For example, if we use 350 and 1000 ppm $\text{CO}_2(\text{g})$ partial pressures in the chambers, we will use 1.3 and 3.6 ppm $\text{H}_2\text{S}(\text{g})$ partial pressures; this is based on the calculations presented in Section 7.2.4 (i.e. $\log(f_{\text{CO}_2} / f_{\text{H}_2\text{S}}) = 2.44$). If we use different $\text{CO}_2(\text{g})$ partial pressures, the $\text{H}_2\text{S}(\text{g})$ partial pressures will change accordingly. As with the carbon dioxide and nitrogen, the overall $\text{H}_2\text{S}(\text{g})$ flow rates will also be very low. The contaminant supply stream from the permeation tube will be below 1000 sccm, and the overall flow rate will be below 4000 sccm.

A series of barriers will be used to ensure that any gas which is released is vented safely. The $\text{H}_2\text{S}(\text{g})$ diluted stream will flow in the chambers containing the samples. The chambers outflow will be vented through a ventilation system, described in the next section. The $\text{H}_2\text{S}(\text{g})$ chambers will be kept in a temperature controlled-incubator. The incubator will be kept in a segregated room of the laboratory, where only H_2S -related work will be performed; this room will feature its own separated ventilation system, as described below.

The H_2S room ventilation system will be reviewed and approved by a SNL Industrial Hygienists, prior to beginning the actual experimental work. The ventilation system does not need to be explosion-resistant, because we will not use explosive concentrations of H_2S .

Several hydrogen sulfide monitors will be installed to warn of any H_2S release; the monitors will be connected to an automatic notification system (i.e. building alarm or automatic paging system), to ensure sufficient warning. The H_2S monitors will be placed as follows: one in the temperature controlled-incubator, one within the H_2S room but outside the incubator, one right outside the H_2S room, and one in the building corridor leading to the laboratory hosting the H_2S room.

The staff working with H_2S is required to wear the appropriate personal protection equipment (PPE):

- Eye protection: Wear splash resistant safety goggles with a faceshield.
- Clothing: Wear appropriate chemical resistant clothing, such as cotton lab coat.
- Gloves: Wear appropriate chemical resistant gloves, made of materials such as butyl rubber, polyvinyl chloride, or neoprene.

Staff must ensure that H_2S is kept from incompatible materials, which are described in the H_2S MSDS.

H_2S will be stored and handled in accordance with all current regulations and standards, as described in the H_2S MSDS. It will be stored in a cool, dark, well-ventilated, and dry place, separated from incompatible materials.

All personnel engaged in working in the laboratory building will be notified of the presence and dangers of H₂S, as well as the measures to be taken in case of H₂S release and personnel injuries due to H₂S.

13.2.3.3 MEASURES AFTER ACCIDENTAL RELEASE

If one or several H₂S alarms are triggered:

1. All personnel must immediately evacuate the laboratory building,
2. The Carlsbad fire department is contacted by dialing 911,
3. The following people are notified: 6822 manager, facility manager, laboratory manager.

In case of inhalation, the person must leave the contaminated area immediately; preferably to go outside the building. The Carlsbad fire department is to be contacted by dialing 911. The person will receive medical attention.

If a staff member is found unconscious in or near the H₂S room of the laboratory, it will be assumed that it is due to H₂S exposure, even if no H₂S alarm was triggered. In such case:

1. All personnel must immediately evacuate the laboratory building,
2. The Carlsbad fire department is contacted by dialing 911,
3. The following people are notified: 6822 manager, facility manager, laboratory manager.
4. No SNL personnel will attempt to enter the H₂S room until it is declared safe by emergency response personnel and approved by 6822 manager, facility manager, and laboratory manager.

In case of skin contact, wash skin with soap and water for at least 15 minutes while removing contaminated clothing and shoes. Get medical attention, if needed. Thoroughly clean and dry contaminated clothing and shoes before reuse.

In case of eye contact, flush eyes with plenty of water for at least 15 minutes. Then contact Carlsbad fire department, dialing 911 to get immediate medical attention. If possible, have a co-worker contacting 911 while flushing the eyes.

In case of large amount ingestion, dial 911 to get immediate medical attention.

13.3 Thermal

There are two thermal hazards associated with this experimentation. The first is the H₂S to SO₂ converter used with the H₂S analyzer. The reactor itself is heated to a relatively high temperature (300 °C) in order to complete the conversion. The reactor is shielded within the equipment case, so there is no risk of accidental exposure during normal operation of the system. The second thermal hazard is represented by the heating mantles used for the gas saturation system. While the normal operating condition is below 40 °C, unforeseen circumstances may result in the temperature rising above this level. As such, signage clearly indicating the potential danger will be used.

13.4 Pressure

All pressure systems will be documented by Pressure Safety Data Packages (PSDPs), which have been reviewed by the Pressure Safety Advisor, as required by the SNL Pressure Safety Manual. (MN471000)

13.5 Readiness Review

Prior to begin the experimental work, a Readiness Review will be implemented, following the Readiness Review Process, as described in Section 13D of the SNL ES&H Manual.

14 PERMITTING/LICENSING

There are no special licenses or permit requirements for the work described in this Test Plan.

Information Only

15 REFERENCES

- ASTM, 2003a. Standard Practice for Conducting Mixed Flowing Gas (MFG) Environmental Tests, ASTM B827-97, American Society for Testing and Materials (ASTM) International
- ASTM, 2003b. Standard Practice for Preparing, Cleaning, and Evaluating Corrosion Test Specimens, ASTM G1-2003, American Society for Testing and Materials (ASTM) International
- Babb, S.C., and C.F. Novak. 1997 and addenda. "User's Manual for FMT Version 2.3: A Computer Code Employing the Pitzer Activity Coefficient Formalism for Calculating Thermodynamic Equilibrium in Geochemical Systems to High Electrolyte Concentrations." Albuquerque, NM: Sandia National Laboratories. ERMS 243037.
- Brush, L.H. 2005. "Results of Calculations of Actinide Solubilities for the WIPP Performance Assessment Baseline Calculations." Analysis report, May 18, 2005. Carlsbad, NM: Sandia National Laboratories. ERMS 539800.
- Brush, L.H., and Y.-L. Xiong. 2003. "Calculation of Organic Ligand Concentrations for the WIPP Compliance Recertification Application." Analysis report, April 14, 2003. Carlsbad, NM: Sandia National Laboratories. ERMS 527567.
- Bull Run Metal. 2004. TRU-Shield™ Lead-Lined Storage Containers. Sandia National Laboratories WIPP Record Center. ERMS 541709.
- Burns, T. 2005. "Estimated Containers in the Waste Isolation Pilot Plant (WIPP) Based on TWBID, Rev. 2.1, Data version 4.15." Analysis Report, January 24, 2005. Carlsbad, NM. Los Alamos National Laboratory. ESRMS# 538501.
- Chivot, J. 2004. *Fonctions Thermodynamiques, Diagrammes de Solubilité, Diagramme E-pH des Systèmes Fe-H₂O, Fe-CO₂-H₂O, Fe-S-H₂O, Cr-H₂O et Ni-H₂O en Fonction de la Temperature.* Collection Sciences et Techniques. Châtenay-Malabry, France: Agence Nationale pour la Gestion des Déchets Radioactifs.
- Choppin, G.R., A.H. Bond, M. Borkowski, M.G. Bronikowski, J.F. Chen, S. Lis, J. Mizera, O. Pokrovsky, N.A. Wall, Y.X. Xia, and R.C. Moore. 2001. *Waste Isolation Pilot Plant Actinide Source Term Test Program: Solubility Studies and Development of Modeling Parameters.* SAND99-0943. Albuquerque, NM: Sandia National Laboratories.
- Cotsworth, E. 2004. Untitled letter with enclosure to R.P. Detwiler with third set of CRA comments and requests for additional information, September 2, 2004. Washington, DC: U.S. Environmental Protection Agency Office of Air and Radiation. ERMS 536771.
- Cramer, S.D. and J.P. Carter., 1980. "Corrosion in Geothermal Brines of the Salton Sea Known Geothermal Resource Area", *Geothermal Scaling and Corrosion, Honolulu, Hawaii,*

- April 4-5, 1979. Eds. L.A. Casper and T.R. Pinchback. ASTM International, Philadelphia, PA.
- Crawford, B.A. 2005a. "Waste Material Densities in TRU Waste Streams from TWBID Revision 2.1 Version 3.13, Data Version D.4.15." Analysis Report, April 13, 2005. Carlsbad, NM: Los Alamos National Laboratory. ERMS 539323.
- Crawford, B.A. 2005b. "Tables Containing Lead Data from TWBID Rev.2-1 D4.15". Memorandum to J. Trone, October 20, 2005. Carlsbad, NM: Los Alamos National Laboratory. ERMS 541735.
- Francis A.J., J.B. Gillow, and M.R. Giles. 1997. *Microbial Gas Generation under Expected Waste Isolation Pilot Plant Repository Conditions*. SAND96-2582. Albuquerque, NM: Sandia National Laboratories.
- Garrels, R.M., and C.L. Christ. 1990. *Solutions, Minerals, and Equilibria*. Boston, MA: Jones and Bartlett.
- Golden, J. 2004a. "Specification for the Fabrication of the Standard Waste Box." Carlsbad, NM: Washington TRU Solutions.
- Golden, J. 2004b. "Specification for the Fabrication of the Ten Drum Overpack." Carlsbad, NM: Washington TRU Solutions.
- Golden, J. 2005. "Specification for the Fabrication of the Standard Large Box 2 (SLB2)." Carlsbad, NM: Washington TRU Solutions.
- Hertelendy, N.A. 1984. *Rockwell Hanford Operations User's Manual for Remote Handled Transuranic Waste Container*. Rockwell International document no. RHO-RE-MA-7, September 1984.
- Kubal, M., F. Panacek. 1995. "Potential-pH Diagram for Fe-H₂O-Citric Acid System," *British Corrosion Journal*. Vol 30, no. 4, 309-311.
- Lide, D.R. 2004-2005. *CRC Handbook of Chemistry and Physics*, 85rd edition. Boca Raton, FL: CRC Press
- Martell, A.E., R.M. Smith, and R.J. Motekaitis. 1998. *Critically Selected Stability Constants of Metal Complexes Database, Version 5.0*. College Station, TX: Texas A&M University Press.
- Molecke M.A. N.R. Sorensen, and G.G. Wicks. 1993. *Waste Isolation Pilot Plant Materials Interface Interactions Test: Papers Presented at the Commission of European Communities Workshop on In Situ Testing of Radioactive Waste Forms and Engineered Barriers*. SAND93-1055. Albuquerque, NM: Sandia National Laboratories.
- Munson, D.E., R.L. Jones, D.L. Hoag, and J.R. Ball. 1987. *Heated Axisymmetric Pillar Test (Room H): In Situ Data Report (February, 1985 - April, 1987)*,

Waste Isolation Pilot Plant (WIPP) Thermal/Structural Interactions Program.
SAND87-2488. Albuquerque, NM: Sandia National Laboratories.

- Nemer, M.B. and J.S. Stein. 2005. "Analysis Package for BRAGFLO: 2004 Compliance Recertification Application Performance Assessment Baseline Calculation." Carlsbad, NM: Sandia National Laboratory. ERMS #540527.
- Nemer, M.B., Stein, J.S., and Zelinski W. 2005. "Analysis Report for BRAGFLO Preliminary Modeling Results with New Gas Generation Rates Based Upon Recent Experimental Results." Carlsbad, NM: Sandia National Laboratories. ERMS 539437.
- Pletcher, D., D. Sidorin, B. Hedges., 2005, "A Comparison of the Corrosion of Carbon and 13% Chromium Steels in Oilfield Brines Containing Acetate." *CO₂ Corrosion in Oil and Gas Production Symposium, Proceedings of the NACE Corrosion/2005 conference, held in Houston, TX, April 3-7, 2005*, National Association of Corrosion Engineers (NACE) International, Houston, TX, Paper no. 05301.
- Popielak, R.S., R.L. Beauheim, S.R. Black, W.E. Coons, C.T. Ellingson and R.L. Olsen. 1983. *Brine Reservoirs in the Castile Formation, Waste Isolation Pilot Plant Project, Southeastern New Mexico*. TME 3153. Carlsbad, NM: U.S. Department of Energy WIPP Project Office.
- Pourbaix, M. 1974. *Atlas of electrochemical Equilibria in Aqueous Solutions*. Houston, TX: National association of Corrosion Engineers.
- Robinson, K.L. 1996. "Preparing Synthetic Brines for Chemical Retardation and Transport Experiments." Unpublished technical operating procedure, TOP-544. Albuquerque, NM: Sandia National Laboratories.
- Saltykov, S.N., G.V. Makarov, E.L. Toroptseva, and Y.B. Filatova. 1989. "Anodic Behavior of White Iron Phases in Oxalic Media." *Protection of Metals*. Vol. 40, no. 1, 56-61.
- Sankarapavinasam, S., F. Pushpanaden, M.F. Ahmed. 1989. "Dicarboxylic Acids as Corrosion Inhibitors for Lead in HClO₄," *Bulletin of Electrochemistry*, Vol. 5, no. 5, 319-323.
- Sankarapavinasam, S., F. Pushpanaden, and M.F. Ahmed. 1989. "Hydrazine and Substituted Hydrazines as Corrosion Inhibitors for Lead in Acetic Acid," *British Corrosion Journal*. Vol. 24, no. 1, 39-42.
- Shukla, J., and K.S. Pitre. 2004. "Corrosion of Carbon Steel in Inhibited Acidic Medium: A New Voltammetric Approach," *Bulletin of Electrochemistry*. Vol. 20, no 7, 309-313.
- Snider, A.C. 2003. "Verification of the Definition of Generic Weep Brine and the Development of a Recipe for This Brine." Analysis report, April 8, 2003. Carlsbad, NM: Sandia National Laboratories. ERMS 527505.

Stein, J.S. 2005. "Estimate of Volume of Brine in Repository That Leads to a Brine Release." Memorandum to L.H. Brush, April 19, 2005. Carlsbad, NM: Sandia National Laboratories. ERMS 539372.

Telander, M.R., and R.E. Westerman. 1993. *Hydrogen Generation by Metal Corrosion in Simulated Waste Isolation Pilot Plant Environments*. SAND92-7347. Albuquerque, NM: Sandia National Laboratories.

Telander, M.R., and R.E. Westerman. 1997. *Hydrogen Generation by Metal Corrosion in Simulated Waste Isolation Pilot Plant Environments*. SAND96-2538. Albuquerque, NM: Sandia National Laboratories.

U.S. Congress. 1992. "WIPP Land Withdrawal Act." Public Law 102-579, 110 Stat. 2422, as amended by 104-201 (1996). Washington, DC: U.S. Congress.

U.S. DOE. 2004. Title 40 CFR Part 191 Compliance Recertification Application for the Waste Isolation Pilot Plant, Vol. 1-8. DOE/WIPP 2004-3231. Carlsbad, NM: U.S. Department of Energy Carlsbad Field Office.

Uhlig, H.H., and R.W. Revie. 1985. *Corrosion and Corrosion Control: An Introduction to Corrosion Science and Engineering*. New York, NY: John Wiley and Sons.

Wall, D. 2005. ES&H Standard Operating Procedure, Activities in the Sandia National Laboratories/Carlsbad program Group Laboratory, Building NPHB (U). SP473548. Carlsbad, NM. Sandia National Laboratories.

Wang, Z., R.C. Moore, A.R. Felmy, M.J. Mason, and R.K. Kukkadapu. 2001. "A Study of the Corrosion Products of Mild Steel in High Ionic Strength Brines," *Waste Management*. Vol. 21, 335-341.

WIPP Performance Assessment Department. 2001a. "Design Document for PAPDB Version 1.00." Carlsbad, NM: Sandia National Laboratories. ERMS 518615.

WIPP Performance Assessment Department. 2001b. "User's Manual for PAPDB Version 1.00." Carlsbad, NM: Sandia National Laboratories. ERMS 518617.

Woolsey, G., 2005. "Lead Lined Drum Projections." Memorandum to N. Wall, October 20, 2005. Carlsbad, NM: Washington TRU Solutions. ERMS 54658.

Xia, Y., L. Rao, D. Rai, and A.R. Felmy. 2001. "Determining the Distribution of Pu, Np, and U Oxidation States in Dilute NaCl and Synthetic Brine Solutions," *Journal of Radioanalytical and Nuclear Chemistry*. Vol. 250, no. 1, 27-37.

NOTICE: This document was prepared as an account of work sponsored by an agency of the United States Government. Neither the United States Government nor any agency thereof, nor any of their employees, nor any of their contractors, subcontractors, or their employees, makes any warranty, express or implied, or assumes any legal liability or responsibility for the accuracy, completeness, or usefulness or any information, apparatus, product or process disclosed, or represents that its use would not infringe privately owned rights. Reference herein to any specific commercial product, process or service by trade name, trademark, manufacturer, or otherwise, does not necessarily constitute or imply its endorsement, recommendation, or favoring by the United States Government, any agency thereof or any of their contractors or subcontractors. The views and opinions expressed herein do not necessarily state or reflect those of the United States Government, any agency thereof or any of their contractors.

This document was authored by Sandia Corporation under Contract No. DE-AC04-94AL85000 with the United States Department of Energy's National Nuclear Security Administration. Parties are allowed to download copies at no cost for internal use within your organization only provided that any copies made are true and accurate. Copies must include a statement acknowledging Sandia Corporation's authorship of the subject matter.

Information Only